Chapter 9

Innovative Theoretical Approaches Used for RF Power Amplifiers in Modern HDTV Systems

Daniel Discini Silveira, Marcos Paulo de Souza Silva,
Marcel Veloso Campos and Maurício Silveira

Additional information is available at the end of the chapter

http://dx.doi.org/10.5772/63547

Abstract

The essential purpose of this chapter is to introduce theoretical and numerical approaches that can be used for modeling nonlinear effects that appear intrinsically in the design of power amplifiers that have been used widely in many modern high-density television (HDTV) architectures. Important effects like the pre-distortion using adaptive techniques, with distinct characteristics like amplitude, phase, and frequency, as well as, their specific nature such as *AM*/*AM*, *AM*/*PM*, *PM*/*AM,* and *PM*/*PM*, and constitute one of the main directions of this research. All theoretical and technological approaches have been supported by a consistent set of numerical data performed with one of the most important platform of simulations used in the great area of Radio Frequency (RF) and Microwave structures. As a direct application, we are introducing some efficient processes that can be used for the characterization of RF systems with a set of consistent laboratorial measures that permit us to visualize the effective cost and a complete architecture for the characterization of high-power amplifiers. With the continuous and innovative technological demand that is imposed by the international marketing has a great importance to find versatile systems that are capable of measuring several amplifier characteristics, as gain, output power, inter-modulation distortion of different signals, efficiency, current, and temperature that constitute another direction of research that has been demanded strongly for news advanced technologies used widely in modern HDTV systems.

Keywords: innovative theoretical modeling, digital pre-distortion, nonlinear power amplifiers, characterization of RF systems, numerical approach, measurement systems, HDTV architectures

1. Introduction

Nowadays, the research and development of the modern *RF* power amplifiers have been demanded some continuous and accurate studies concentrated over the linearity of the equipment. Besides the distortions caused by the nonlinear devices, we have been having a constant improvement in the implementation of new modulation techniques by exploring the spectrum properties [1]. The nonlinear performance caused by the devices is a fundamental effect, which have invoked the attention of many researchers in many famous research centers around the entire world [2, 3]. In Section 2, we will focus our research in the development on an adaptive prototype for the linearization of the power amplifier with resources of the digital pre-distortion, in a such way that it is possible to generate a feedback distortion through the power amplifiers [4, 5]. This will provide a much more linear final answer, being the main application applied for modern high-density television (*HDTV*) transmitter equipment. In the current literature, we can classify this type of pre-distortion as being adaptive, since that we will must to compare the input signal with that transmitted one, which it includes the distortion generated by the power amplifier [6]. The theoretical as well as experimental approach starts by set an open-loop prototype until to reach the closed loop by adopting an adaptive system for analog signals, such that the digital treatment uses the adaptive techniques over the entire transmission system [7–14].

Actually, for many modern implementations of broadcast TV transmitters, the association of power amplifiers (PAs) is performed in order to obtain the desired output power, usually higher than 1 kW. The filtered output signal is expected to present low levels of distortion, so it does not interfere in adjacent broadcast channels. A signal applied to a power amplifier (PA) will suffer from distortions, independently of its input level and the technology (BJT and LDMOS) [1, 2, 15]. Basically, three types of distortions are caused in the input signal: amplitude, frequency, and phase. Amplitude distortions are caused by the amplifier gain compression, P_{1dB}, a device-dependent characteristic. By clipping, the signal harmonics are generated, also classified as frequency distortion. The magnitude of these harmonics is increased with the amount of signal clipping, consequently increasing the overall distortion. Phase distortions are mainly caused by memory effects present in amplifiers due to the different reasons, as biasing, transistor transit-time, thermal effects, and others. Operating the amplifier in significant *back-off* can avoid some of these undesirable distortions, but the efficiency of the amplifier will be very poor. A powerful way to decrease distortion in the output signal is to use linearization techniques, thus operating the PA in a more efficient way [16–18]. Some initial research for the *AM*/*AM* analysis can be obtained, by imposing that the transfer function of the output voltage of the power amplifier had third-order nonlinear dependence with respect to the input signal. Although the numerical approach adopted in that occasion was efficient for this particular case, the nonlinear effect for the *AM*/*PM* analysis was not compensated [19–22]. Example of models which can compensate these and also other distortions can be found with a study over several practical models. An accurate model is the first step for the implementation of an efficient pre-distortion system using a parallel model has obtained good results, compensating for both *AM*/*AM*, *AM*/*PM* distortions, and also for memory effects, the

main causes of distortions in the PA output signal. These main theoretical and experimental approaches constitute the most important contributions presented in the Section 3 [23, 24–26].

During these last years, a wide class of theoretical approaches have been presented for the current literature that involves the project of the power amplifiers modeled with field-effect transistor (*FET*) structures, where the main focus is concentrate over the linear region of the device [2–5, 27–29]. Recently, important studies were done for nonlinear microwave circuits as well as the new design for wireless digital structures. Also some innovative studies using linearization techniques with high gain of the power amplifiers, as well as the great importance it acquires the presence of an active pre-distortion circuit for monolithic microwave integrated circuit (*MMIC*) components implemented with field-programmable gate array (*FPGA*) architectures [30–32]. More recently, a set of innovative research appears in the current literature, with the introduction of a new theoretical modeling for the nonlinear analysis of the power amplifiers, where the electronic structure modeling was strongly motivated by the involvement of the authors with the project of modern HDTV equipments. With respect to industrial implementations, this research has an expressive contribution related with polarization of the digital structures using the common source configuration in the design of all hybrid RF circuits [33]. Therefore, the desired great stability can be reached independent of the particular pre-distortion that must be corrected in the real time, like: *AM*/*AM*, *AM*/*PM*, and all the others cases. The theoretical approach presented in the Section 4 can be used for a wide class of modern power amplifiers independent of the particular modulation system that will be adopted for the design of the HDTV systems. Some experimental measurements are performed, and we make a comparison with all numerical simulations using a very powerful numerical platform, that is, the Advance Design Systems (*ADS*) that confirm all ours theoretical approaches [34, 35].

The characterization of RF power systems or products over the entire Ultra High Frequency (*UHF*) band is very difficult and sometimes expensive task that demands time and accuracy. This means expensive and specialized setups capable of performing the necessary measurements [36–45]. In Section 5, we present a high performance and low-cost setup designed for test and characterization of RF high-power amplifiers, capable of generate reports that will help the operator to decide about the conformity of the equipment with other ones tested, as we can see in the characterization of a power drawer [46–52]. The drawer is composed by four power amplifiers, capable of delivering a maximal output power of 860 Watts peak sync (Wps), 430 (W) for the USA digital TV broadcast system (*ATSC*), or 220 (W) for the standard adopted in the Japanese/Brazilian systems (*ISDB-T*). The architecture presented in this section can naturally also be used to characterize other RF power amplifiers, where the power drawer was only a particular case.

2. Efficient experimental techniques to control the adaptive linearization: digital signals *I* and *Q*

In this section, we intend to focus the implementation of an efficient FPGA electronic architecture than can serve for those systems that have a very sensible characteristic, with respect

to the nonlinear distortions [1]. In principal, this research will be directed for the analysis of both *I* and *Q* complex signals in order to minimize both *Phase* (*AM-PM*) and *Amplitude* (*AM-AM*) distortions that are present intrinsically in the functioning of the architecture. One of the most important steps to be conquered with this design is to combine the power amplifier with a digital pre-distortion system, in order to get an acceptable inter-modulation level at the output.

With respect to the numerical implementations, all programs are made using classic computational methods, such as *linear correlation* and *linear regression*, which are very convenient for this kind of distortion as well as permits for the designer to work close to the linear operation region of the amplifier [2–5].

2.1. Fundamental relationships adopted for the linear numerical approach

Recently, the implementation of innovative electronic architectures that involve numerical implementation has an important requirement to investigate the relationship existent between two or more variables presented in the system. The verification of the degree of relationship between the variables is object of the correlation studies, with the essential purpose to measure and to evaluate the relationship existent between two random variables [6–8].

Typically, the linear correlation seeks to measure the relationship between the variables and through the disposition of the points around a straight line and is used exhaustively for the determination of the correlation coefficient. For a more general computational modeling, we must to detect the correlation that exists between two arbitraries variables. For that case, it is possible to allocate all points over a straight line, which corresponds the known classic method of the linear correlation, while the points in the two-dimensional real domain must be placed close of some curve and establish a nonlinear correlation.

If both variables *x* and *y* have the same characteristics such that the increase of the first variable must impose the same performance for the second one, we are in front of the positive linear correlation, where the alternative case is corresponding to the negative linear correlation. The perfect linear correlation happens when the points *x* and *y* are perfectly aligned. The null correlation occurs when there is not a relationship among the variables, which implies that all variations can happen independently [9–12].

The linear coefficient, α_r, which in the international literature is known as the Pearson correlation can be described by Eq. (1) in the analytic form:

$$|\alpha_r| = \frac{\sum_{i=1}^{n} |(x_i - \bar{x})(y_i - \bar{y})|}{\sqrt{\sum_{i=1}^{n}(x_i - \bar{x})^2 \sum_{i=1}^{n}(y_i - \bar{y})^2}} \tag{1}$$

http://dx.doi.org/10.5772/63547

In the previous equation, we have: n = number of pairs (x, y); $\bar{x}$ and $\bar{y}$ = averages of both x and y variables. The coefficient α_r has values in the interval I = [−1, 1] that corresponds the correlation level, as is illustrated in **Table 1**.

Amplitude	Correlation level
$\lvert\alpha_r\rvert = 0$	Zero
$0 < \lvert\alpha_r\rvert \leq 0.30$	Weak
$0.30 < \lvert\alpha_r\rvert \leq 0.60$	Medium
$0.60 < \lvert\alpha_r\rvert \leq 0.90$	Strong
$0.90 < \lvert\alpha_r\rvert < 1$	Very strong
$\lvert\alpha_r\rvert = 1$	Perfect

Table 1. Amplitude of the parameter α_r.

The proximity of the parameter α_r close to zero permits us to identify that there does not exists a significant linear correlation between the variables x and y, while if this coefficient is close to ±1, we can conclude that there exists a strong correlation. Typically, for the general case, we have: $0 \leq \lvert\alpha_r\rvert \leq 1$.

The straight line of the minimum square that adjusts the set of points $\{(x_1, y_1), (x_2, y_2), \ldots (x_n, y_n)\}$ that has a better adjustment performed through the linear equation:

$$y = a.x + b \tag{2}$$

For this numerical approach, the constants a and b can be determined by solving the normalized system composed by the equations:

$$a = \frac{\sum_{i=1}^{n}[(x_i - \bar{x}).(y_i - \bar{y})]}{\sum_{i=1}^{n}(x_i - \bar{x})^2} \quad b = \bar{y} - a.\bar{x} \tag{3}$$

2.2. An initial hardware implementation

In order to reach the demanded linearization, we must to take into account some very important parameters, such as operation frequency, the temperature, and other ones. It is great to emphasize that those parameters are not constant as a function of the time, and thus we must to set their control under an adaptive digital system.

If our project has the technological demand to work with a fast control and the system must to operate in real time, we looked for to substitute the used memory for a model implemented

experimentally by a *Programmable Logic Device* (*PLD*) just because its present some countless advantages. In our case, we have opted for a *Look-Up Table* (*LUT*) digital architecture.

The analog video signal is transformed in a digital one that proceeds for the *LUT* and for the retard circuit, aiming to establish the best relationship among the samples. In other words, we must to get a better synchronism, and at that point, the adjustment algorithm compares the samples of the correlator and the *up-date-algorithm* will make the updating at the *LUT*.

An initial architecture for the pre-distortion system can be visualized through the block diagram shown in **Figure 1**. Despite of we have many parameters to adjust, has a great importance the fact that we still must to be sure that we have comparing the samples in the same instant of time. A program can be developed in C++ language to control the whole system, and this initial idea proved to us a great effectiveness in the linearization as well as in the correction of the amplitude.

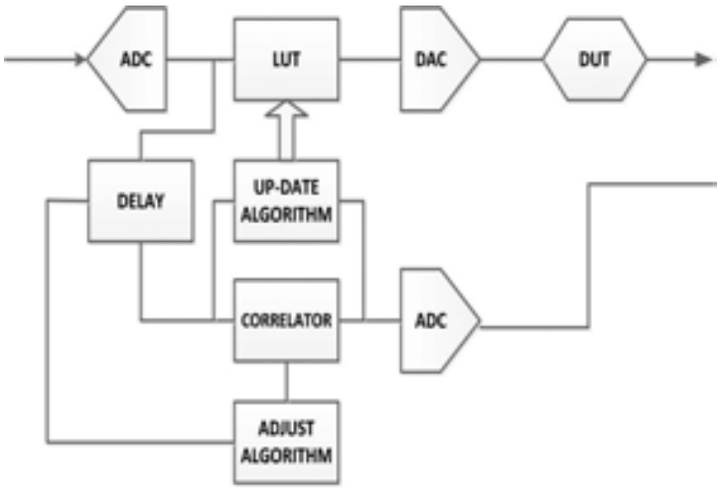

Figure 1. Block diagram: digital pre-distortion system.

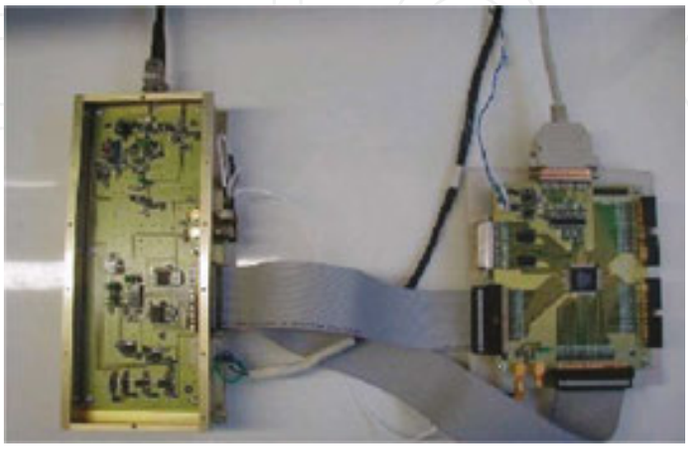

Figure 2. An initial hardware architecture: pre-distortion system.

At the same time, our hardware implementation must be projected as well as operate with distinct input digital signals: *I* (*Phase*) and *Q* (*Quadrature*), such that it is possible to correct both amplitude and the phase of each one. An initial whole architecture for the Module of Programmable Logic (*MLP*), the *PLD* plate and the converters, can be visualized in **Figure 2**. At first, the control is done through the C++ software; but with the progress of this project, it is possible to set the control through a device that make the digital signal processing (*DSP*), as well as making the use of a microcontroller, by placing him in the same architecture besides both *AD* and *DA* converters.

2.3. An improvement of the hardware architecture

The linearization of the signals has a great importance, because independently of the distinct *TV* digital patterns that have been adopted in many countries, the systems have a very sensible characteristic with respect to the nonlinear distortions. These effects always have been demanding the need of to implement circuits that can provide an efficient linearization [9–15].

With respect to the analysis of both *I* and *Q* complex signals, the new linearizer circuit must allow to get a better performance for the whole architecture. In order to minimize both *Phase* (*AM-PM*) and *Amplitude* (*AM-AM*) distortions, the ideal solution would be to combine the power amplifier with a digital pre-distortion system, in order to get an acceptable intermodulation level at the output. In this project, we concentrate our choice over the *FPGA* electronic architectures.

2.4. Experimental measurements in accordance with a set of compatible simulations

At first, it is important to emphasize that the *FPGA* architecture works like a *LUT* that stores the input data and permits to establish a comparison between all of them with the coming set of feedback data. At the same time, this comparison is performed; the numerical codes inserted inside the digital architecture shall supply to the *LUT* a new set of values that can be stored, being this process a constant and continuous routine.

For the flow of the data inside the entire architecture, we can use the *Matlab* platform, for the generation of the input signal with *two tones* [10–12]. This function can be accomplished by the first *FPGA* structure, and in the sequence, we can pass the signal through the pre-distortion processor. The output signal will enter in the second *FPGA* architecture that has the essential function of to simulate the power amplifier. After the amplification is performed, we can remove the feedback signal that will be compared with that one to be transmitted, and as one direct consequence, it is possible to realize all corrections that are demanded by the project in both signals.

An update of the first architecture exhibited previously can be visualized in **Figure 3**.

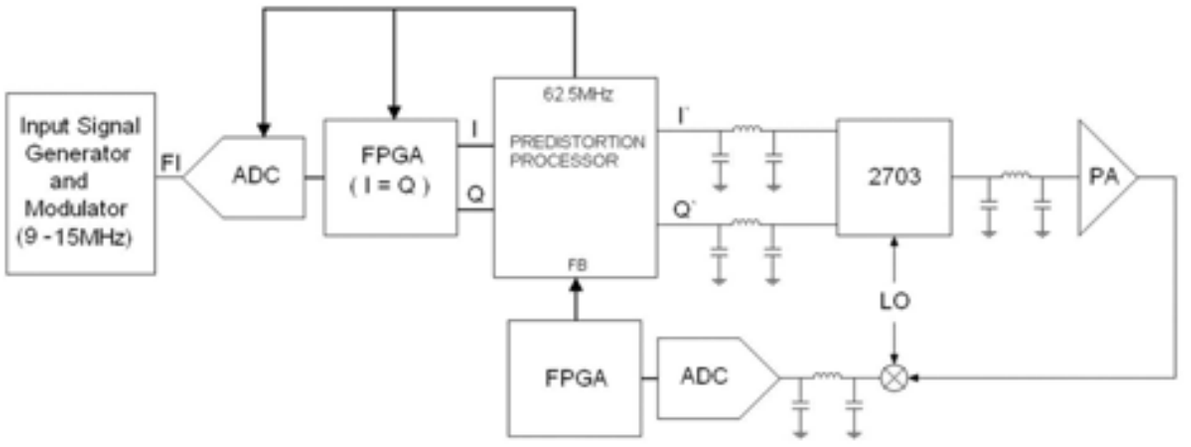

Figure 3. An improvement of the first hardware architecture.

In **Figure 4(a–c)**, we can visualize the input signal, the distorted signal by the amplifier and the error vector, respectively, and the error vector corresponds to the subtraction of the two previous signals at the same time t.

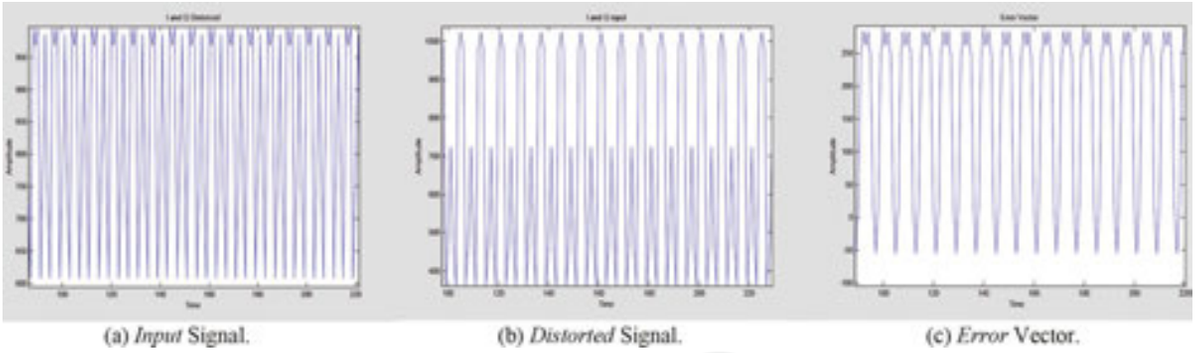

Figure 4. Some of the most important signals detected in some points of the architecture, plotted with the *MatLab* as a function of the time t (s). (a) *Input* Signal. (b) *Distorted* Signal. (c) *Error* Vector.

The *linear regression method* combined with *linear correlation* using the *FPGA* technology permits to adjust the linear function $y = f(x) = ax + b$. A reverse effect for the distortion is shown in **Table 2**, using as a numerical approach the inverse linear function $x = g(y) = (1/a).[y - b]$, where the parameters a and b are defined as in Section 2.1, where evidently we are presenting all numerical data placed in distinct lines.

For this case, if we consider the entire set of ideal values, all coefficients defined in Section 2.1 acquire the values: $\bar{x} = 48.5$, $\bar{y} = 48.39$, $a = 1.1837$ and $b = -9.02$. In addition, in **Figure 5**, it is possible to visualize the transition of the most important curves with respect to the ideal linear performance of the amplifier, by adopting this numerical approach for the adaptive pre-distortion linearization.

http://dx.doi.org/10.5772/63547

y ideal	40	41	42	43	44	45	46	47	48
x up-date	41.4	42.2	43.1	43.9	44.7	45.6	46.4	47.3	48.1
y ideal	49	50	51	52	53	54	55	56	57
x up-date	49.0	49.8	50.7	51.5	52.4	53.2	54.0	55.0	55.8

Table 2. *Up-Date* of the input signals.

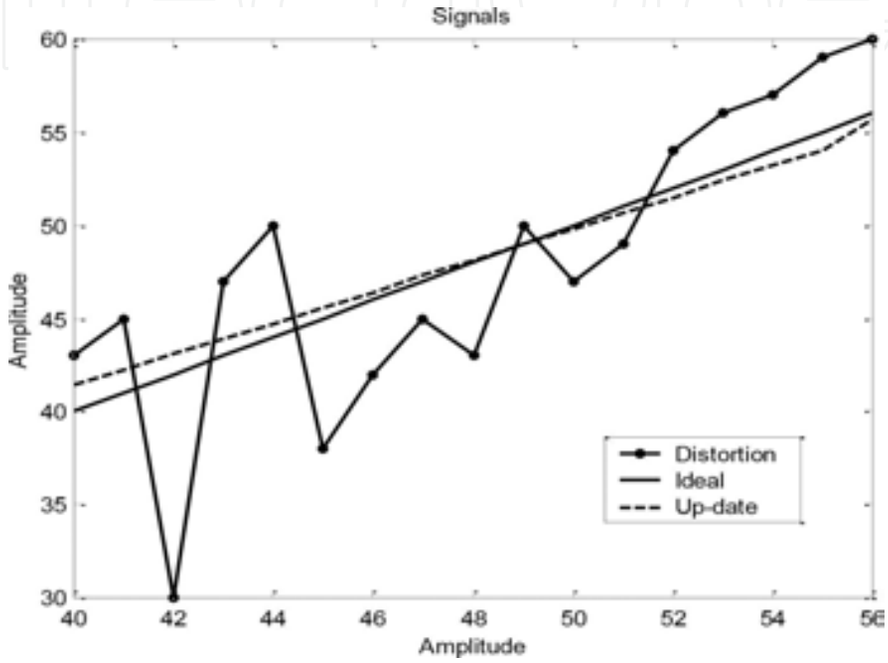

Figure 5. An improvement of the hardware architecture.

Figure 6 is presenting one of the most important *FPGA* architecture used for all experimental measurements.

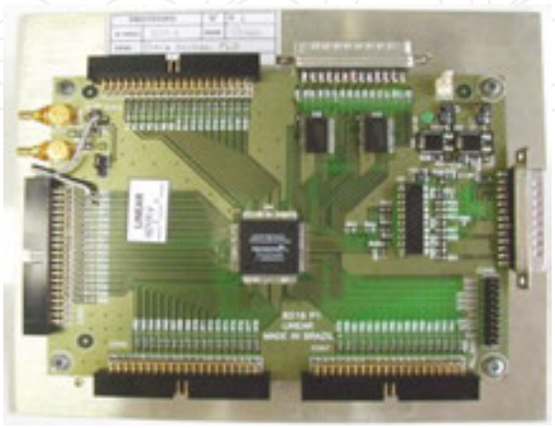

Figure 6. One FPGA programmable logic module architecture.

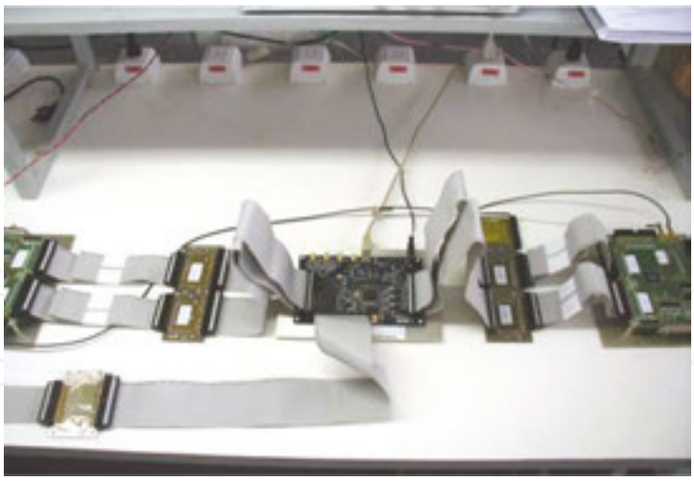

Figure 7. The entire pre-distortion digital architecture.

Finally, in **Figure 7**, we are showing the entire architecture implemented for experimental tests of a modern HDTV transmission equipment. In this Section, we present a programmable logic module architecture that have as the main function to control the linearization process, which permits for us to acquire more knowledge about how to set the programming codes more easily [13–15].

It is easy to confirm the nonlinear performance of the power amplifiers provokes the harmonic distortion as well as the inter-modulation products as a function of how many carriers we have used for setup the system. This apprenticeship permits for the designer to get more background with the linearization approaches and uses an appropriate software for the adaptive digital pre-distortion techniques.

3. Distortions for *ISDB*-T OFDM signals for RF power amplifiers architectures

The essential purpose of this Section is to present some recent development for many types of digital modulations, capable of transmitting large amount of data, which occurs for the standard *ISDB-T*. For this case, the carrier combination can generate a reasonable number of voltage spikes in the time domain, depending of its phase.

Experimentally, some important parameters like the figure of merit, the peak-to-average ratio (PAR), assume an important role with respect to improve our background of how to determine the level of the compression point of 1 (dB) for a wide class of AB power amplifiers. Depends on how efficient is the architecture will be implemented, it is possible to confirm that a large back-off of all amplifiers used in the *ISDB-T* transmitter chain needs to be performed, in comparison with the case of an analog broadcast transmission.

Normally, the gain compression is caused by inter-modulation characteristics of the transistors, with major influence of the third harmonic component. The inter-modulation distortion

(*IMD*) can be easily measured when more than one carrier is used as a PA input signal, as two tones with equal amplitude. For the case that a two-tone test signal is applied to an amplifier, it is possible to observe several inter-modulation components at the output spectrum generated due to the transistor nonlinear behavior.

For an *ISDB-T* standard Orthogonal Frequency Division Multiplexing (OFDM) signal with thousands of carriers, the distortion at the fundamental zone appears as a set of multiple distortions, and the bandwidth of the distortion is related to the signal bandwidth. Therefore, it is possible to establish some relationships between the signal bandwidth with the second and higher-order distortions for a specified fundamental frequency for the system. In addition, it is possible to detect the fundamental zones that corresponding to odd or even distortions, and some of them can be removed using filters [17, 19, 23].

Another set of important parameters and effects must be controlled for a system with memory, such as low (high) frequency, thermal effects, trapping effects, biasing circuits, Automatic Gain Control (*AGC*) loops; transistor (transit time and parasitic reactance), matching networks (group delay). The amount of memory is defined as the time between the origin of the kernel until the point where it passes through zero and is directly dependent of the transmitted signal bandwidth.

Some particular cases can be analyzed for RF power amplifiers in order to get more information about general classification of memory effects, in linear and nonlinear ones, as well as the *memoryless* systems. Thus, it is possible to confirm the origin of linear memory and that the nonlinear memories are generated in the nonlinear dynamic interactions of the input signal. Another important experimental procedure confirms that a practical PA output signal has both linear and nonlinear memory, and an *ISDB-T* OFDM signal that occupies a fixed bandwidth with up to thousand of carriers will cause more memory effects in a PA than for an analog signal, which has a small number of carriers [20–22, 24].

3.1. Fundamental principles over the clipping and inter-modulation distortion effects

Generally, there are many types of digital modulations, capable of transmitting large amount of data. If the OFDM technique is used, the signal can contain thousands of carriers. Depending of the phase of these carriers, the combination can result in a signal with high *Crest Factor*, demanding very high output power from the system PA. The system will be then inefficient.

It is possible to quantify the magnitude of this *Crest Factor* by the following equation, named here peak-to-average ratio (PAR), defined by:

$$PAR = 20.Log(|X_{PEAK}|/X_{Av}) \tag{4}$$

where X_{PEAK} and X_{Av} are the maximum and the average values (V) of the signal, respectively. The X_{PEAK} value can be quantified by an oscilloscope with enough bandwidth to measure the signal in time domain. The X_{Av} can be measured using a Wattmeter, and later converting this value to voltage, assuming a 50 (Ohms) load. The PAR from some common used signals is: 3

(dB) for a continuous wave (CW), 3.5–4 (dB) for a *QPSK*, and approximately 12 (dB) for the *ISDB-T* standard OFDM.

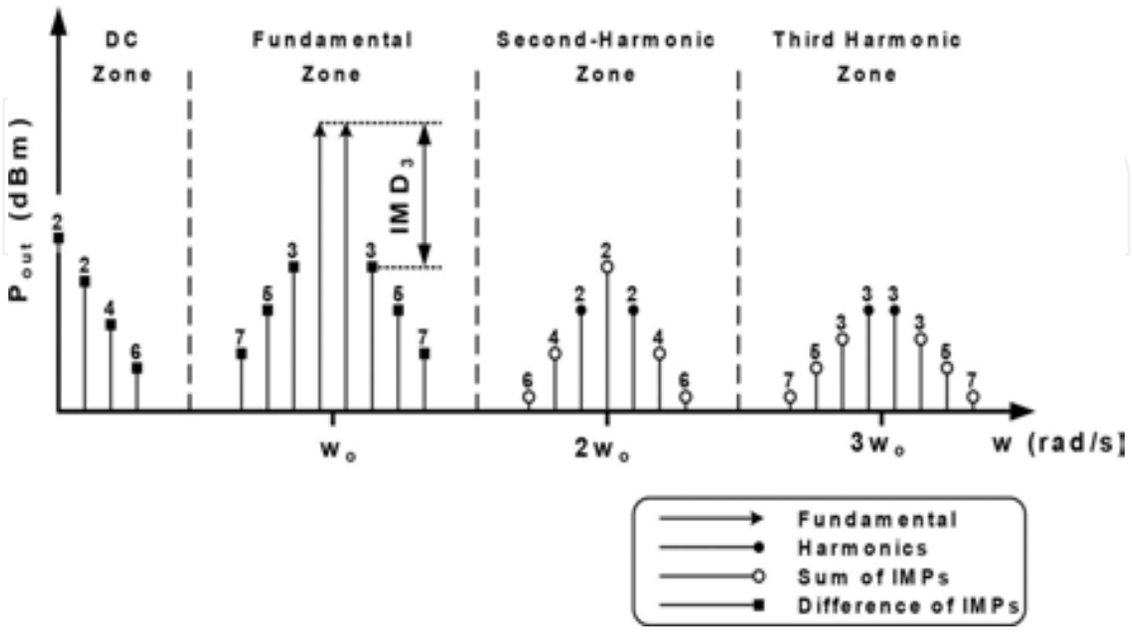

Figure 8. Several components of inter-modulation generated by a *two-tone* test signal applied to a PA.

Inter-modulation can be easily measured when more than one carrier is used as a PA input signal, as two tones with equal amplitude. When a *two-tone* test signal is applied to an amplifier, it is possible to observe several *IMD* components at the output spectrum generated due to the transistor nonlinear behavior, as seen in **Figure 8**.

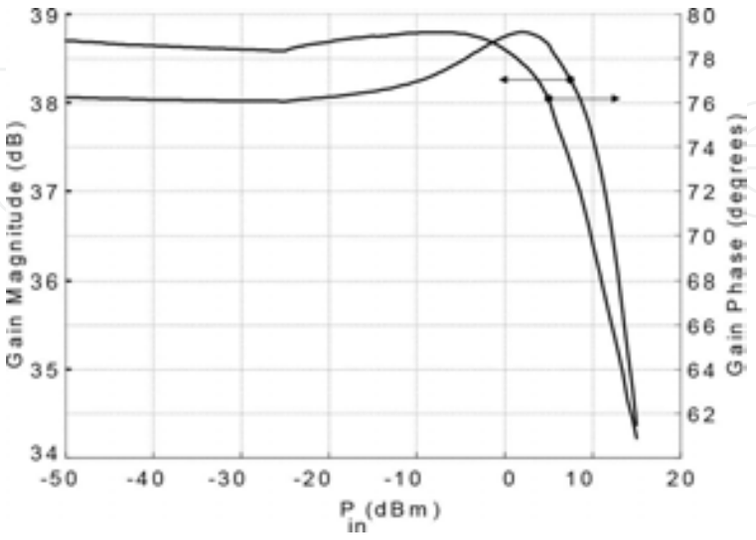

Figure 9. Typical gain curve of a class AB power amplifier.

http://dx.doi.org/10.5772/63547

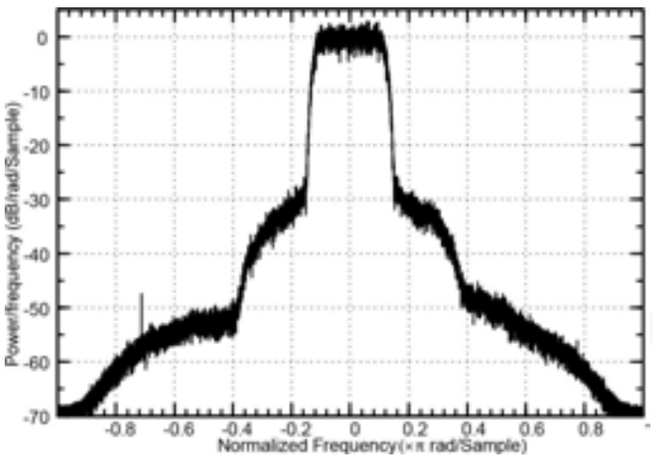

Figure 10. Distortion generated by a PA when excited by an *ISDB-T* standard signal.

By adopting this procedure, if a class AB PA has a compression point of 1 (dB) at 10 (*dBm*), as shown in **Figure 9**, an OFDM signal in the *ISDB-T* standard can be amplified until a maximum input power of −2 (*dBm*), using this PA, without compression of the signal peaks. Therefore, a large *back-off* of all amplifiers used in the *ISDB-T* transmitter chain needs to be performed, in comparison with the case of an analog broadcast transmission. The gain compression is caused by inter-modulation (IMD) characteristics of the transistors, with major influence of the third harmonic component.

In an *ISDB-T* standard OFDM signal with thousands of carriers, the distortion at the fundamental zone appears as a set of multiple distortions, as in **Figure 10**. The bandwidth of the distortion is related to the signal bandwidth. Thus, if a signal has a bandwidth of 5.6 (MHz) at the fundamental frequency, the bandwidth of the second-order distortion will be of (2)*(5.6) = 11.2 (MHz), the third-order distortion will have bandwidth of (3)*(5.6) (MHz), and so on. The odd-order distortions lie inside the fundamental zone, requiring a different treatment than the even order ones. These lie outside the fundamental and at the DC zone, and can be removed using filters.

A possibility to avoid IMD occurrence is to perform *back-off*, as said before. This procedure obviously increases costs in the transmission system, due to an increased number of PAs, but will guarantee a very high quality of the transmitted *ISDB-T* signal, measured by the MER in (dB), which excellent levels are over 40 (dB). On the other side, if high values of *back-off* are used, the PA efficiency is affected, as the amplifier will operate with less power than it was designed for. Therefore, a careful trade-off between *back-off*, or high values of MER, and PA efficiency has to be carefully established.

3.2. About the intrinsic dependence of memory effects

A system with memory is that one where the output signal has dependency of past states of the input signal. The memory of a system can be estimated through the observation of the first-order *Volterra* kernel. The amount of memory is defined as the time between the origin of the

kernel until the point where it passes through zero and is directly dependent of the transmitted signal bandwidth.

Let us consider the particular case of a RF power amplifier, which has a complex structure and presents many kinds of memory. For our experimental procedure, we adopt the classification in accordance with the band of frequencies, in the form:

A. *Low frequency* (kHz to MHz): Thermal effects, trapping effects, biasing circuits, AGC loops.

B. *High frequency* (GHz): Transistor (transit time and reactance parasitics), matching networks (group delay).

These memories are mixed together in a nonlinear coupled power amplifier, and the problem of estimating behavioral models becomes very difficult. A general classification of memory effects, in linear and nonlinear ones, can be found, while the *memoryless* system is characterized if the output signal envelope follows the variations of the input signal envelope.

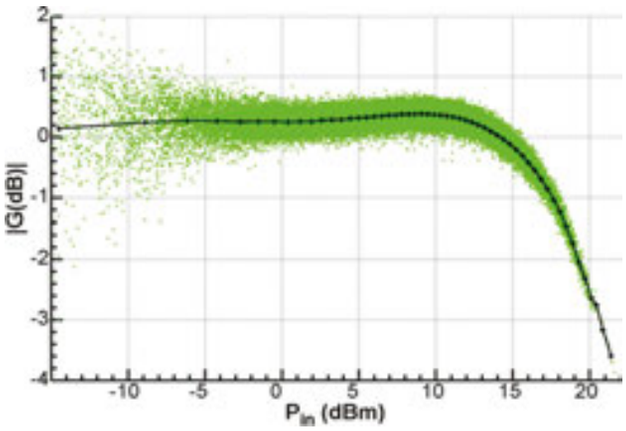

Figure 11. Plot of an *AM/AM* characteristic curve. The center line illustrates an estimate of the *memoryless* amplifier behavior.

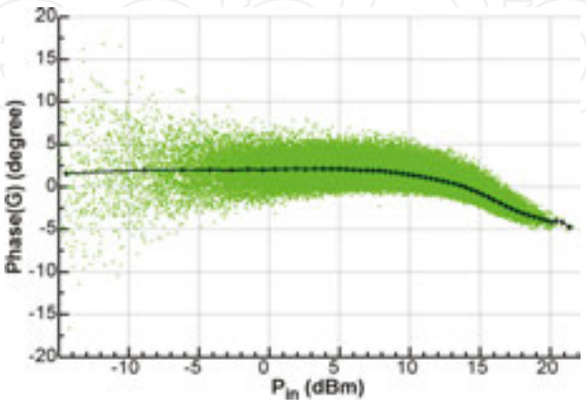

Figure 12. Plot of an *AM/PM* characteristic curve. The values close to the origin at the abscissas axis may include some errors of synchronization as well as measurement noise.

http://dx.doi.org/10.5772/63547

Matching networks are the origin of linear memory, and nonlinear memories are generated in the nonlinear dynamic interactions of the input signal. A practical RF PA output signal has both linear and nonlinear memory, and an *ISDB-T* OFDM signal that occupies a bandwidth of 5.7 (MHz) with up to 8.000 carries will cause more memory effects in a PA than an analog signal, which has only three carriers.

The effects caused by a system with memory in a signal can be easily viewed through *Amplitude*/*Amplitude* (*AM*/*AM*) in **Figure 11** and *Amplitude*/*Phase* (*AM*/*PM*) in **Figure 12**, where the central line shows a *memoryless* amplifier behavior. The spreading of points for a particular instantaneous power indicates more memory, although close to the origin at the abscissas axis may include some errors of synchronization as well as measurement noise also. These plots were obtained from time-domain measurements performed by a Vectorial Signal Analyzer (*VSA*). Another memory definition can be found in the literature that permits to include a "*time*" interval between "*AM*/*AM* and *AM*/*PM* curves".

The IMD effects mixed with memory effects of a PA can generate distortions that degrade seriously the output signal, which can make the task of achieving the required ISDB-T norm mask more difficult. As every amplifier presents distortion, the only way to produce cost-effective and efficient amplifiers is to implement methods to compensate or correct these distortions, as presented in next section.

3.3. Correction of distortions and the technology of the compensation methods

Distortions caused in the amplitude of a signal can be corrected basically with *back-off*, the simpler, and the less-efficient method. If linearization is used, many methods can be applied. The most frequently used ones are *feed forward* and *pre-distortion* with pros and cons listed in our initial references [16, 17, 19, 20, 23].

Choosing the right model is the key for the compensation experimental techniques to control a wide class of distortions generated intrinsically by the RF power amplifier. An efficient architecture for experimental measurements can be built using a basic platform that allows the simulation several models together with *ISDB-T* OFDM signal generation. The board architecture includes essential devices such as *A*/*D* and *D*/*A* converters, a FPGA architecture which realizes the *Mux* and *Demux* for *Trelis-Encoder* and *Reed-Solomon* digital communications, memories, and other circuits, as we are presenting in **Figure 13**.

A fundamental step surpassed for the hardware architecture setup implementation was the construction of a filter with excellent sideband attenuation, like surface acoustic Wave (*SAW*) filters that normally present problems regarding pass-band ripple, high insertion loss, and high cost. Using the FPGA and DSP techniques and digital filters, this problem was solved. In addition, it was also possible to compare two distinct theoretical and experimental approaches: *Weaver* and *Frequency Complex* methods combined with DSP techniques, which permit to generate *AM-VSB* analog TV and *8-VSB* digital TV signals through a simplified architecture [6, 7, 8, 23, 25, 26].

This *FPGA* structure was used to implement the nonlinear experimental approach discussed in this chapter and to achieve the best results for the pre-distortion. This architecture was

designed, implemented, tested and was in industrial production, part of the first transmission HDTV equipment in Brazil for the *ISDB-T* standard and the electronic structure can serve also for other standards of modulation.

Figure 13. The implemented architecture used to check both theoretical and experimental approaches.

The approach discussed in this Section reveals different distortions that occur in an RF PA input signal, specifically the *ISDB-T* OFDM signal, and their main sources. Further on, common compensation methods were discussed: *back-off*, linearization using *feed forward*, and pre-distortion, including costs involved in each method. For the design of a good quality, efficient, and cost-effective transmitter, a careful study about the distortion generated by the RF amplifier has to be performed. The architecture was designed such that the pre-distortion methods were implemented in practice, and the correct compensation method can be chosen, in order to obtain the highest efficiency allied to high quality [7–9, 14, 17, 23, 25, 26].

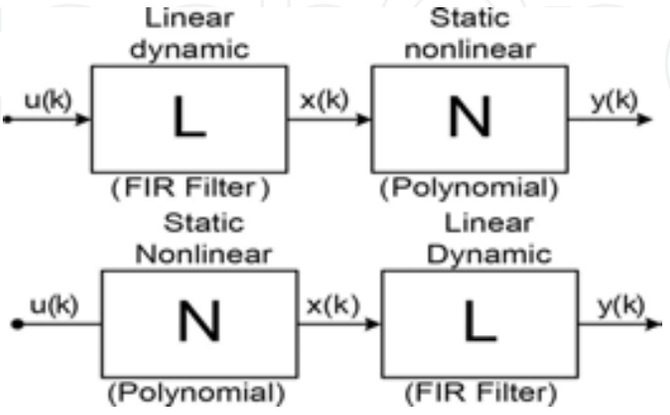

Figure 14. Examples of models including linear and nonlinear blocks. The *Wiener* model contains a filter before the nonlinearity block, and the *Hammerstein* model has the nonlinear block first.

http://dx.doi.org/10.5772/63547

By considering the fact that only those models that include memory in their architectures can be effective against the distortions generated by the modern RF PAs, **Figure 14** presents an example of a block diagram proposed by *Wiener* and *Hammerstein*. Normally, this approach can be adopted in accordance with the compensated distortion that varies as a function of the imposed bandwidth and also with the complexity of the adopted pre-distortion structure.

4. An innovative nonlinear technological modeling of RF power amplifiers for HDTV architectures

The essential purpose of this section will be to present an efficient theoretical approach for modeling with high precision power amplifiers that have quadratic characteristics for both input voltage and the output current. Although our approach will refer for the *FET* device, the same ideas can be adopted for the others structures such as *MOS*, *LDMOS*, and other similar ones. Through the entire section, we will assume that the signal is working in the active region of the transistor, which implies that the input voltage V_{gs} is bigger than the threshold V_t. Some particular cases can be analyzed, if we use the Fourier approach for modeling the drain current of the device [2–5, 15, 21, 28]. In order to compare our experimental results with our technological approach, all computational simulations will be performed using the most important numerical platform for this special kind of nonlinear analysis, which is the software *Advanced Design System* (*ADS*), that permits to show with high-resolution harmonic spectrum for any output signal.

In order to get a more complete idea of this theoretical approach, we must to consider the presence of signals of great amplitudes, such that it is possible to detect the occurrence of the saturation of the device as well as in some cases this effect can occurs abruptly. For that case, the more convenient modeling that can be adopted is to use a partial quadratic characteristic with multiple segments. Therefore, we must to extend our initial analysis for the Fourier series that represents a *pulse train* with distinct sinusoidal peaks for the amplitudes of the currents.

The last theoretical modeling permit us to make the calculations of the coefficients of the Fourier cosine series for all respective train of pulses, which turns out in the new series obtained with the coefficients we have found in the previous analysis. This study is strongly supported if we have enough involvements with new power architectures, just due to the fact that these equipments have some enormous requirements imposed over the project of all hybrid circuits in order to get more stability in the analysis for both *AM*/*AM* and *AM*/*PM* digital pre-distortion corrections on real time. The *ADS* platform permits to make to visualize the harmonic components of higher order, such that all numerical results can be compared with those ones that we can get with our hardware implementation.

Our technological approach will be tested with the experimental data that we can exhibit with the project of an electronic architecture that was built at the Laboratory of HDTV Systems of a Company that have a wide class of power amplifiers in this line of industrial production. This device was designed for validation our theoretical approach in order to get a complete

set of experimental measurements, and the RF Amplifier was implemented using a *LDMOS MRF 9060* component.

4.1. Quadratic behavior of the *FET* transistor

We start by assuming that we have a quadratic characteristic between both input voltage and output current that can be approached with a good precision for a *FET* device, such that an input tension V_{GS} can control a current source I_d [15, 28–30]. In this case, we will have a quadratic behavior of the type:

$$I_d(t) = \frac{I_{DSS}}{V_T^{\,2}}(V_{GS} - V_T)^2, \quad V_{GS} = V_b + V_1.\cos\omega.t \tag{5}$$

where I_{DSS} = Intrinsic parameter of the transistor, V_T = Threshold voltage, V_{GS} = Gate to source voltage, V_b = Bias tension, and V_1 = Peak tension. We can assume always the signal is working in the active region of the transistor, which implies that the input signal V_{GS} is bigger than the threshold one V_T, with $V_x = V_T - V_b$. Therefore, we combine the previous definition, and we can derive in the equation:

$$I_d(t) = \left(\frac{I_{DSS}}{V_T^{\,2}}\right).\left(\frac{V_1^2}{2} + \frac{V_1^2.\cos 2.\omega.t}{2} - 2.V_1.V_x.\cos(\omega.t) + V_x^{\,2}\right) \tag{6}$$

It is easy to verify that an expansion in Fourier series for $I_d(t)$ has only three terms, and they are:

$$I_d(t) = I_0 + I_1 cos\omega.t + I_2 cos 2.\omega.t \tag{7}$$

If we compare the expression expanded in (6), with the *Fourier* series shown in (7), it is easy to check that:

$$I_0 = \frac{I_{DSS}}{V_T^{\,2}}\left(V_x^{\,2} + \frac{V_1^2}{2}\right), \quad I_1 = -2.\frac{I_{DSS}}{V_T^{\,2}}V_x.V_1, \quad I_2 = \frac{I_{DSS}}{V_T^{\,2}}\frac{V_1^2}{2} \tag{8}$$

To check the efficiency of this approach, we consider an analytical model with the following set of parameters: I_{DSS} = 16 (mA), V_t = −4 (V), V_b = −2 (V), and V_1 = 2.cos($4.\pi.10^{\,7}t$) (V). Thus, if we make the calculations in accordance with the Eq. (6), the current I_d (t) in (mA) can be done by:

$$I_d(t) = [6 + 8\cos(4\pi.10^7 t) + 2\cos(8\pi.10^7 t)] \tag{9}$$

http://dx.doi.org/10.5772/63547

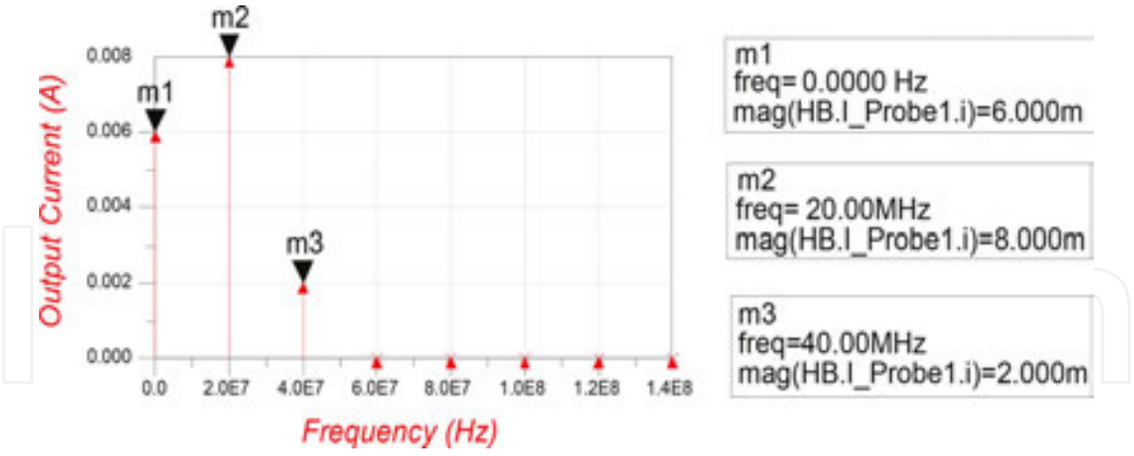

Figure 15. *Amplitude* versus *Frequency* of the output current signal.

Figure 15 shows the harmonic spectrum of the output signal using the software *ADS*. In this case, it is easy to detect that there is a very good agreement between the results obtained with the simulations and those ones obtained with the calculation for the analytical model proposed in this chapter.

In **Figure 16(a)**, we are showing all equipments used in the hardware implementation with the essential purpose of making the validation of the characteristic quadratic of the amplifier presented in this subsection. The graphic shown in **Figure 16(b)** depicts the output current signal, where we are showing into detail the spectral components of first and second order.

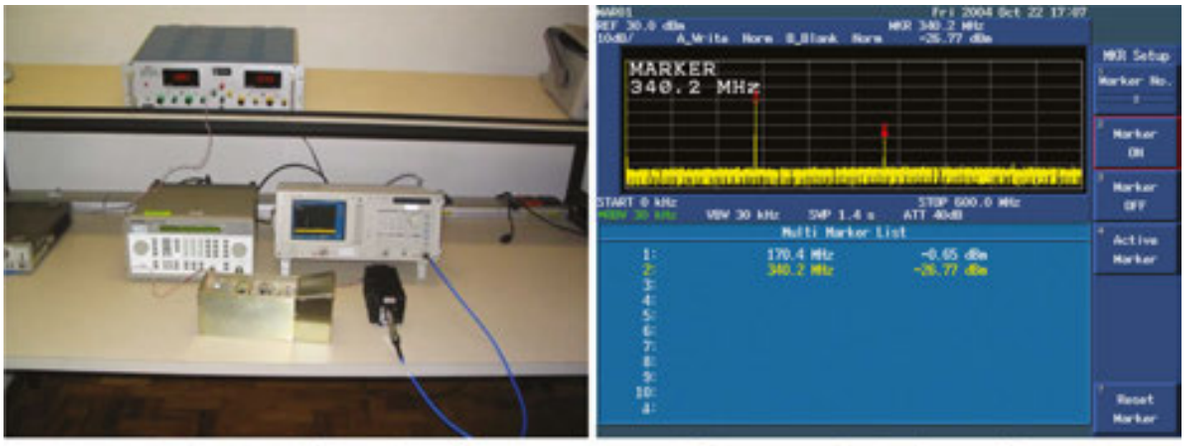

(a) Equipments used for experimental measures. (b) Output current signal of the amplifier.

Figure 16. The architecture designed for experimental measurements—power RF amplifier. (a) Equipments used for experimental measures. (b) Output current signal of the amplifier.

4.2. An innovative analytical approach in the presence of the saturation effect

Typically, in the presence of great signals, it is possible to detect the occurrence of the saturation, and in some cases, this can occurs abruptly. In this case, the more convenient modeling

will be to use a partial quadratic characteristic with multiple segments, and we can adopt the same approach of Section 4.1, such that V_y and V_x are the maximum and minimum limits for the fluctuation of the signal. Starting on the Fourier cosine series, this modeling can be found by the direct subtraction of the series that represents a pulse train with sinusoidal peaks of amplitude I_{p1} and I_{p2}.

In addition, if the conduction angles are $2\varphi_1$ and $2\varphi_2$, we can get a new series where the coefficients are corresponding to the subtraction of those ones of the original Fourier series of each pulse train. Now, if we assume the quadratic behavior of the device and by imposing some limits of fluctuation over the signal, we can express the peak current and the drain currents of the device through the analytical expressions in the form:

$$I_{p1} = \frac{I_{DSS}}{V_T^{\,2}}(V_1 - V_x)^2, \quad I_{d1} = \frac{I_{DSS}}{V_T^{\,2}}(V_1 \cos \omega.t - V_x)^2, \quad \varphi_1 = \cos^{-1}\frac{V_x}{V_1} \tag{10}$$

$$I_{p2} = \frac{I_{DSS}}{V_T^{\,2}}(V_1 - V_y)^2, \quad I_{d2} = \frac{I_{DSS}}{V_T^{\,2}}(V_1 \cos \omega.t - V_y)^2, \quad \varphi_2 = \cos^{-1}\frac{V_y}{V_1} \tag{11}$$

In this case, the Fourier cosine series as a function of θ has the following representation:

$$f(t) = a_0 + \sum_{n\ 1}^{\infty} a_n \cos n.\omega.t, \quad f(t) = I_d(t), \quad a_0 = \frac{1}{\pi}\int_0^{\pi} f\left(\frac{\theta}{\omega}\right).d\theta, \quad a_n = \frac{2}{\pi}\int_0^{\pi} f\left(\frac{\theta}{\omega}\right).\cos(n.\theta).d\theta \tag{12}$$

If we develop the Fourier series for both I_{d1} and I_{d2} currents, where the index j is associated with the current I_{dJ} that must to be determined. Therefore, for $j \in \{0, 1\}$, the iterative process will have the following steps:

$$I_{(J)0} = \frac{I_{pJ}}{\pi}\int_0^{\varphi_J}\left(\frac{\cos\theta - \cos\varphi_J}{1-\cos\varphi_J}\right)^2.d\theta \Rightarrow I_{(J)0} = \frac{I_{pJ}}{\pi}.\frac{\varphi_J - \frac{3}{4}\sin 2\varphi_J + \frac{\varphi_J}{2}\cos 2\varphi_J}{(1-\cos\varphi_J)^2} \tag{13}$$

$$I_{(J)1} = \frac{2.I_{pJ}}{\pi}\int_0^{\varphi_J}\left(\frac{\cos\theta - \cos\varphi_J}{1-\cos\varphi_J}\right)^2.\cos\theta.d\theta \Rightarrow I_{(J)1} = \frac{2.I_{pJ}}{\pi}.\frac{\frac{3}{4}\sin\varphi_J - \varphi_J\cos\varphi_J + \frac{1}{12}\sin 3\varphi_J}{(1-\cos\varphi_J)^2} \tag{14}$$

$$I_{(J)n} = \frac{2I_{pJ}}{\pi}.\frac{(4-n^2).\sin(n\varphi_j) + (3n).\sin[(n-2)\varphi_j] + (n-1).(n-2).[\sin(n\varphi_j).\cos 2\varphi_j]}{(n).(n^2-1).(n^2-4).(1-\cos\varphi_j)^2}, n \geq 2 \tag{15}$$

Finally, we can obtain the iterative current expressed analytically through the equation:

http://dx.doi.org/10.5772/63547

$$I_{d_j}(t) = I_{(j)0} + \sum_{n=1}^{\infty}[(I_{(j)n}).\cos(n.\omega.t)] \tag{16}$$

In addition, we can make the calculations for the coefficients of the Fourier series for both pulse trains that permit to obtain a new series with the subtraction of the coefficients found in the Eq. (16), and represented by:

$$I_d(t) = [(I_{(1)0}) - (I_{(2)0})] + \sum_{n=1}^{\infty}[(I_{(1)n}) - (I_{(2)n})].\cos(n.\omega.t) \tag{17}$$

In order to get more legitimacy of the analytical approach here proposed, we make a comparison similar to that one realized in the previous model. In this second model, we adopt the following characteristics for the device: I_{DSS} = 16 (*mA*), V_x = −4 (*V*), V_y = 4 (*V*), V_b = *0* (*V*), and V_1 = 5.cos(*4.π.10* ^{7}*t*) (*V*). The output current for this case has the spectrum depicted in the **Figure 17(a)**, and all simulations done with the *ADS* software permit us to visualize the harmonic components of higher order. By making a comparison in **Figure 17(b)**, we present a Table where we can detect a very good agreement between the results obtained with the simulation and those ones established with the theoretical modeling that indicates this approach is very efficient and can serves as a tool in the designs of the RF amplifiers. Our professional experience confirms for us that the technological modeling proposed in this subsection can serve for a wide class of projects that involve many modern transmission equipments, with this continuous and rigorous demand imposed by the international market.

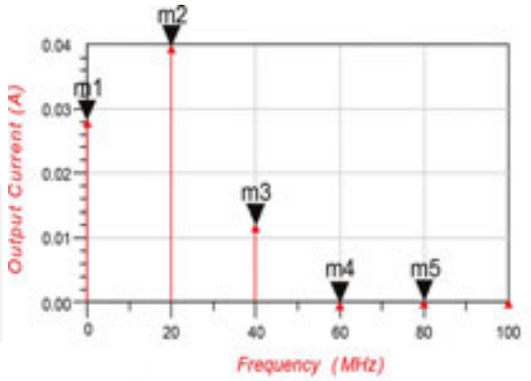

(a) *Amplitude* versus *Frequency* of the output current.

Harmonics	Analytical model	Simulation
DC	28.18 (*mA*)	28.32 (*mA*)
1st (Harmonic)	40 (*mA*)	39.94 (*mA*)
2nd (Harmonic)	12.1 (*mA*)	12.14 (*mA*)
3rd (Harmonic)	10 (*μA*)	64.71 (*μA*)
4th (Harmonic)	264 (*μA*)	361.3 (*μA*)

(b) Analytical Model and the Results of Simulation.

Figure 17. Analytical and numerical analysis of the saturation effect for the power RF amplifier. (a) *Amplitude* versus *Frequency* of the output current. (b) Analytical model and the results of simulation.

In conclusion, **Figure 18** presents some photos of the device implemented in the laboratory of the Company [7–14, 25–26, 34–35, 40]. In the item (a), we shows the zoom of the *RF* Amplifier built using the *LDMOS* MRF 9060 transistor, while that in the item (b), we present a complete view of the electronic architecture that was used for all experimental measurements that were presented into detail in **Figure 16(b)**.

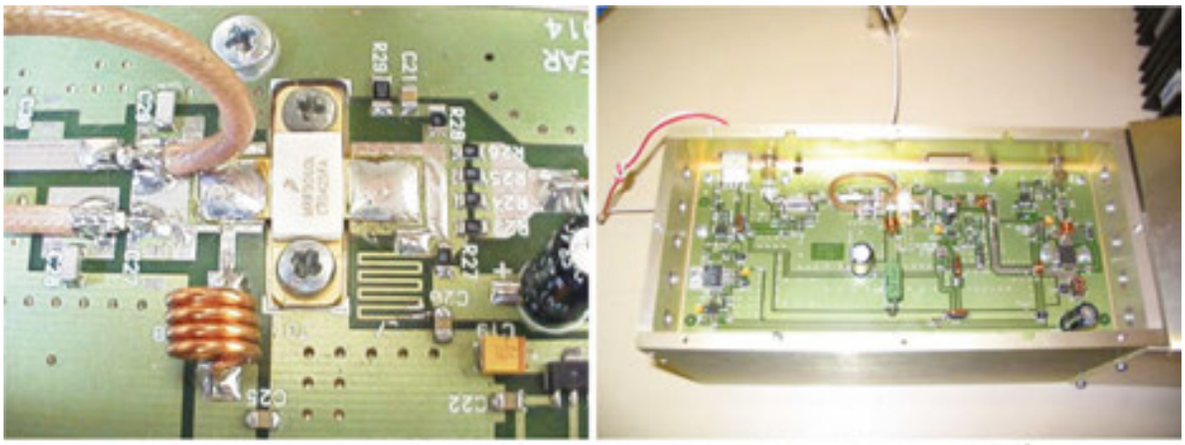

(a) The *LDMOS 9060* Electronic Structure. (b) Power RF Amplifier (*10 W*) at the 3rd band.

Figure 18. Photographs of the hardware architecture for the power RF amplifier. (a) The *LDMOS 9060* electronic structure. (b) Power RF amplifier (*10 W*) at the 3rd band.

4.3. An appropriate theoretical approach for the amplifier with a source resistance

This approach starts by assuming that we will concentrate our analysis over the source resistance effect for the circuit depicted in the **Figure 19**. In this case, we must to get all analytical equations that describe the functioning of the model, and in consequence, it is possible to check that the V_{in} tension cannot be applied directly in the gate-source voltage V_{GS}. Therefore, only part of the voltage appears in the gate-source input of the FET and the complementary tension must be applied in the resistance R. Therefore, in this case, the equ. (18) presents the analytical dependence between these parameters, described analytically in the form:

$$V_{in} = V_r + V_{GS} = (I_d).R + V_{GS} \tag{18}$$

In accordance with the previous studies done by Cantrell and Davis, we can define the input incremental resistance expressed mathematically by:

$$r_{in(n)} = \left(\partial V_{in} \big/ \partial I_d\right)_{I_d = I_{DC}} \Rightarrow r_{in(n)} = \left\{\frac{\partial}{\partial I_d}[(I_d).R]\right\} + \left[\frac{\partial V_{GS}}{\partial I_d}\right] \tag{19}$$

where I_d and I_{DC} are, respectively, the drain and the DC currents defined by the circuit polarization. Starting on the equation that defines the classic modeling of the FET structure, and after some algebraic calculations, it is possible to express the voltage V_{GS} in the form:

$$V_{GS} = \left(I_d \big/ k\right)^{1/2} + V_T, k = \left(\frac{1}{2}\right).(k.n).\left(W \big/ L\right) \tag{20}$$

Under these hypotheses, if we combine conveniently the last equations, both the incremental resistance and the new transconductance can be expressed by the equations:

$$r_{in(n)} = \left(\partial V_{GS} \big/ \partial I_d\right)_{I_d = I_{DC}} = \left(\frac{1}{2.k}\right).\left(I_{DC} \big/ k\right)^{-(1/2)}, g_{m(n)} = \left(\frac{1}{r_{in(n)}}\right)\left[\frac{g_{m(n)}}{1+(g_{m(n)}).R}\right] \quad (21)$$

For a fixed value of the parameter g_m, Eq. (21) shows that the new transconductance decreases as a function of the resistance R. In particular, if the factor $(g_m).R >> 1$, in the limit condition, this expression will depends only of R. Therefore, the transconductance is independent of any change in the polarization current, that is: $g_{m(n)} = 1/R$.

4.4. Additional performance with respect to the effect of the feed-forward linearity

With the final purpose of to get a more knowledge about the effect of the feed-forward linearity, when the electronic structure has the presence of the passive component R, it acquires a great importance define a new curve of transconduction V_{in} versus I_d [3–5, 10–15, 18, 28–30]. This will demand a new modeling in the initial Eq. (18), using the voltage V_{GS} as in Eq. (20), which derives in the expression:

$$V_{in} - V_T + V_{GS} = (I_d).R + \left(I_d \big/ k\right)^{1/2} \quad (22)$$

where V_T is the threshold voltage. This will demand a new definition of the voltage V_c, that indicates the dependence of V_{in} with respect to V_T, when the drain current vanishes, that is $I_d = 0$. Therefore, we can get:

$$V_c = (I_{DC}).(R + r_{in}) \Rightarrow V_c = \left(\frac{I_{DC}}{g_m}\right).[1 + (g_m).R] \quad (23)$$

In order to simplify the 2D plot analysis of the new transconductance, we normalize the Eq. (5) by the voltage V_c as a function of the parameter $(g_m).R$, which imply that:

$$\left(\frac{V_{in} - V_T}{V_c}\right) = \left(\frac{I_d}{I_{DC}}\right).\left(\frac{(g_m).R}{1+(g_m).R}\right) + \left(I_d \big/ I_{DC}\right)^{1/2}.\left(\frac{2}{1+(g_m).R}\right) \quad (24)$$

4.5. Analysis in the limit condition at the presence of the feed-forward effect

At first, in **Figure 20**, we are portraying a graphic that we obtain for three different values of the parameter $(g_m).R$. Therefore, it is possible to check the change in the quadratic curve with respect to the correspondent linear behavior of the amplifier, as well as the decreases of its

gain. Some particular cases related with the real transition of the parameter $(g_m).R$ can be performed, and each one of them has a very simple mathematics derivation, if we look the previous equation at the limit condition.

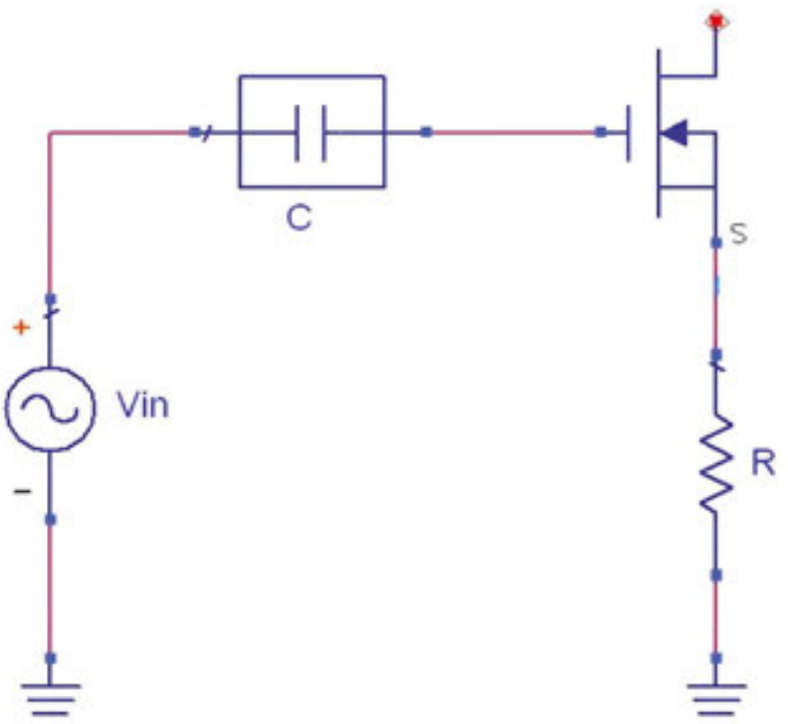

Figure 19. The FET device with the presence of the source resistance.

- At first, it is easy to check that when $(g_m).R << 1$, the behavior of the structure has a quadratic performance.
- For the case that $(g_m).R >> 1$, we will have a linear dependence that involves all variables.
- It is important to emphasize that the limit condition, that is: $(g_m).R = 0$, characterizes the quadratic behavior too, which corresponds exactly the same one presented by the FET device.
- By the other hand, the 2nd limit condition, that is: $(g_m).R \rightarrow \infty$, can be reached with the linear behavior which will be analyzed in the next subsection, more specifically in the set of Eqs. (28) and (29), and is associated to the *threshold* condition of the amplifier.
- Generally, we must to concentrate our approach by making an appropriate choice on the cases discussed in the previous items. The almost linear dependence that corresponds to the limit condition $(g_m).R = 1$, is shown in **Figure 20**.
- Finally, it is important to put in evidence that the case $(g_m).R = 0$, can be solved with those analytical expressions that permits us to detect the quadratic behavior of the FET transistor.

http://dx.doi.org/10.5772/63547

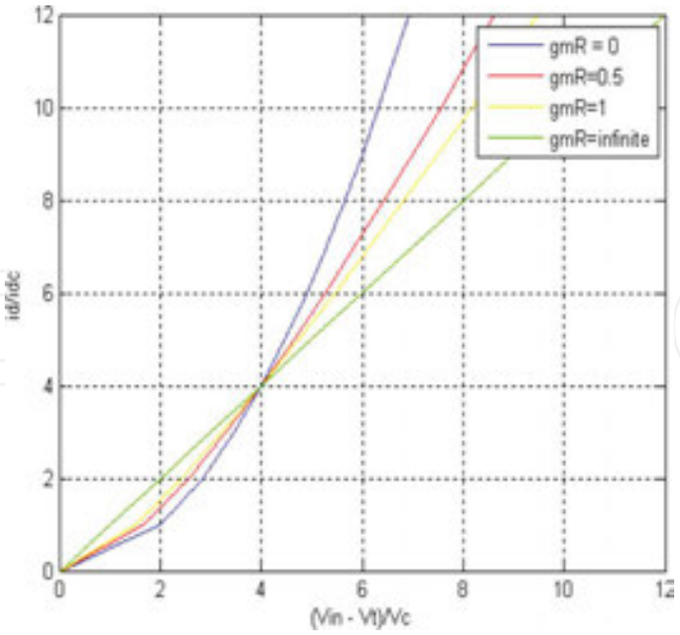

Figure 20. The 2d plot of the transconductance as a function of $(g_m).R$.

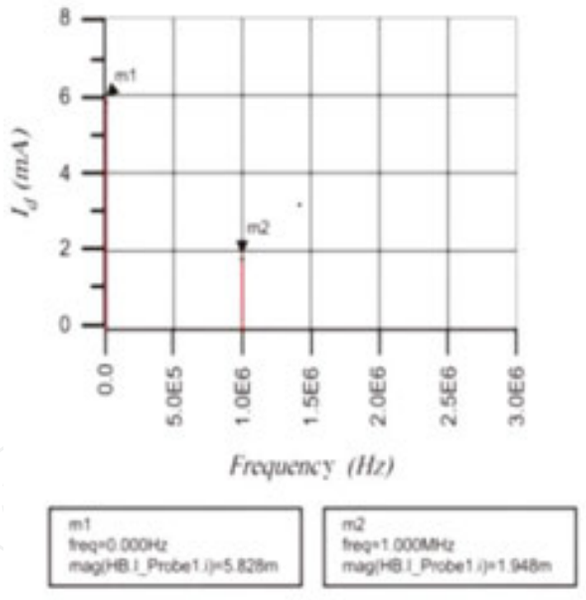

Figure 21. The I_d harmonic components plotted with the *ADS* platform, for $V_{in} < V_c$.

4.6. An important analysis corresponding to the presence of the threshold effect

The threshold condition, $(g_m.R) \rightarrow \infty$, imposes for us focus our analysis over the equation: $I_d = (V_{in} - V_T)/R$, for $V_{in} > 0$, and we will assume that the electronic structure has a voltage source $v_{in} = V_{in}.\cos(\omega.t)$ In this case, two different and important conditions must be analyzed that are as follows:

I. $V_{in} < V_c$—It is easy to check that, if we combine this inequality with the addition condition: $V_c = (I_{DC}).R$, we can assume the linear performance of the FET, which make possible to derive the analytical expression: $I_d = I_{DC} + [V_{in}/R]. \cos(\omega.t)$.

In order to verify the higher dependence of the parameter R, we imposed in our simulations the following set of parameters for the FET structure: $g_m = 86$ (mS), $I_{DC} = 5{,}8$ (mA), $R = 500$ (Ω), and $v_{in} = 1.\cos.[(2\pi.10^6).t]$ (V). For this fixed value of R, we can obtain the transconductance g_m of the amplifier as well as its corresponding polarization, and with this particular choice of the parameters, the more convenient real dependence can be formalized with the following condition: $(g_m).R = 43$.

In addition, the current output I_d characterizes the linear behavior of the amplifier, that is: $(g_m).R >> 1$, and the drain current has the form: $I_d = (5.8) + 4.\cos(\omega.t)$, with $\omega = 2.(\pi).10.\exp(6)$. **Figure 21** depicts the harmonic composition of the output current I_d, simulated with the "*Premium Version*" of platform of simulations: *Advanced Design Systems—ADS* (*Agilent Tech. Co.*). It is possible to confirm that the level of the fundamental component is reduced with the same rate that the transconductance increases. The same comparison can been performed in the case of the quadratic behavior of the FET, if we observe that the 2nd harmonic component does not exist practically, that characterizes the *feed-forward effect*, and this is one of the main reasons we can detect a small reduction in the fundamental component.

II. $V_{in} > V_c$—In this case, the current I_d takes the form of a periodic train of pulses with sine peaks, which can be visualized on **Figure 22**. Then, we must to modeling the device using the classical Fourier Cosine Series.

With respect to the drain current, we can write this signal in accordance with its series representation in the form:

$$I_d(t) = I_0 + I_1 \cos \omega.t + I_2 \cos 2.\omega.t + ... \tag{25}$$

which has an alternative analytical written as:

$$I_d(t) = I_0 + [1 + (I_1 / I_0) \cos \omega.t + (I_2 / I_0) \cos 2.\omega.t + ... \tag{26}$$

If we use this Fourier Cosine Series approximation and we make an accurate analysis over the graphic presented in the **Figure 22**, it is possible to derive the functional dependence like: $I_p = G[V_{in} - [V_{in} - V_T]$. Now, by assuming that $(g_m).R >> 1$, if we follow the same line of ideas we have made previously, we can deduct that $G = g_{m(n)} = (1/R)$, which implies that we will obtain $I_p = (1/R).V_T$.

In the sequence, after some extensive calculations, we can derive the harmonics components for the output signal, using the Fourier series approach, and the set of equations that is possible to derive can be synthesized in the form:

http://dx.doi.org/10.5772/63547

$$\left(\frac{I_n}{I_0}\right)=\left(\frac{2.[\cos\varphi.sen(n.\varphi)-n.sen\varphi.\cos(n.\varphi)]}{n(n^2-1)(sen\varphi-\varphi.\cos\varphi)}\right),\left(\frac{I_1}{I_0}\right)=\left(\frac{\varphi-sen\varphi.\cos\varphi}{sen\varphi-\varphi.\cos\varphi}\right) \tag{27}$$

$$\left(\frac{V_{in}}{V_c}\right)=\left(\frac{\pi}{sen\phi-\varphi.\cos\varphi}\right),\ \varphi=\arccos\left(\frac{V_{in}-V_T}{V_{in}}\right) \tag{28}$$

For some application, we will adopt the same set of parameters used at the end of the last subsection. For this case, we use the input voltage: $V_{in} = 4\ (V)$, since that the condition $V_{in} > V_c$ must be verified. In addition, through the Eqs. (27) and (28), it is possible to determine all harmonic components; and for this next example, we intend to preserve the relation: V_{in}/V_c = 1,372.

It is important to emphasize that, we will obtain a transcendental equation, which demands intrinsically a numerical approach to get the solution in the form: I_d = [5,8 + 7,13.cos.($2\pi.10^6.t$) + 0,696.cos.($4\pi.10^6.t$) + 0,458.cos.($6\pi.10^6.t$) + 0,234.cos.($8\pi.10^6.t$)]. For all numerical simulations, we can explore the resources of the ADS *software* to verify the veracity of the proposed analytical model presented in this section, and the results for the harmonic component of the drain current I_d are depicted in **Figure 23** [32–35].

A comparison between the theoretical and the simulated results is presented in **Table 3** and it is possible to see a small difference between the results determined for the current I_0. To justify these differences, we observe that we have a limitation with respect to the harmonic components involved in the simulation, which not only can provoke some alterations but also has some consequences due to the fact that these values are exceeding the voltage $V_{DC} = 15\ V$.

Harmonics	Analytical model	Simulation
DC	5.8 (mA)	6.13 (mA)
1st (harmonic)	7.13 (mA)	7.22 (mA)
2nd (harmonic)	696.0 (μA)	467.2 (μA)
3rd (harmonic)	458.0 (μA)	363.2 (μA)
4th (Harmonic)	234.0 (μA)	196.8 (μA)

Table 3. Comparison between theoretical and numerical results: harmonics components.

As a direct consequence, the output signal reaches the cutoff region. Furthermore, if the output signal operates outside the cutoff region, intrinsically it can be cut, due to the limits previously established for the excursion of the signal. **Figure 24** presents the output waveform that can reach at maximum the V_{DC} level.

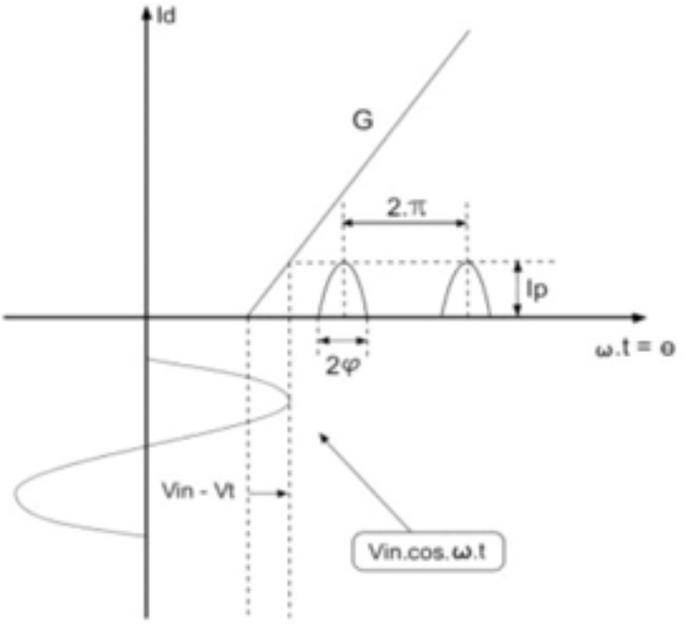

Figure 22. Graphic of the transconductance at the condition: $V_{in} > V_c$.

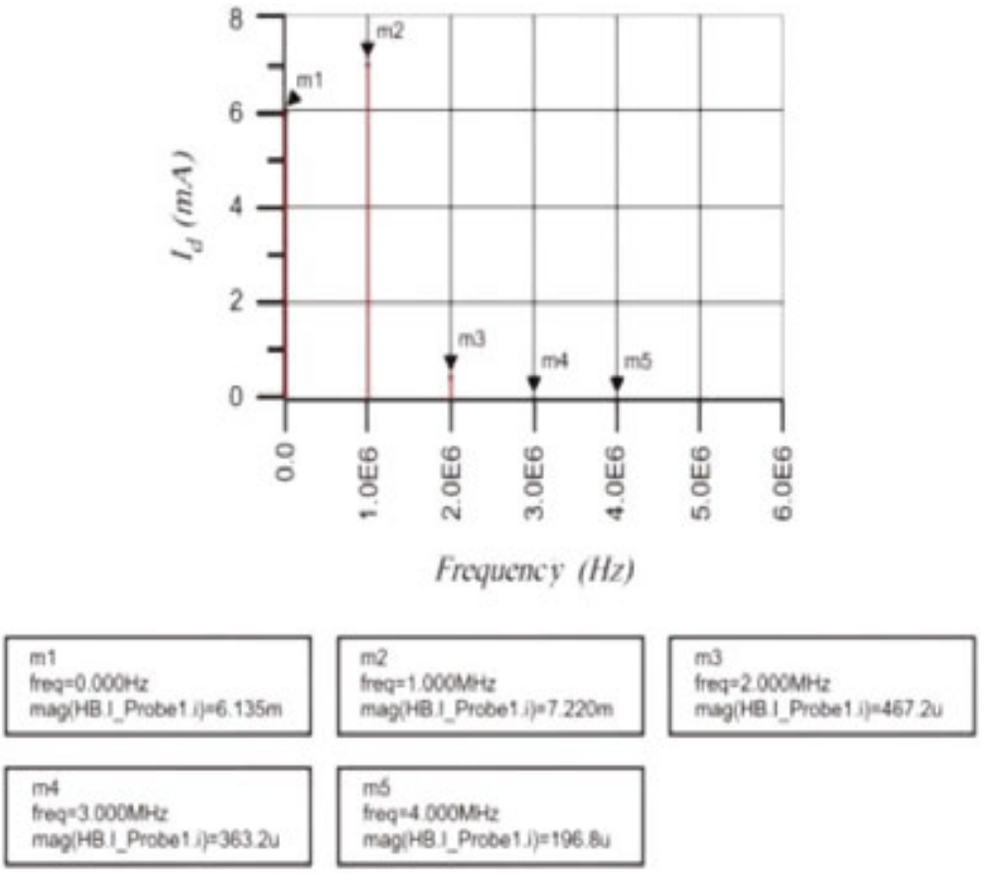

Figure 23. The I_d harmonic components plotted with the *ADS* platform, for $V_{in} > V_c$.

http://dx.doi.org/10.5772/63547

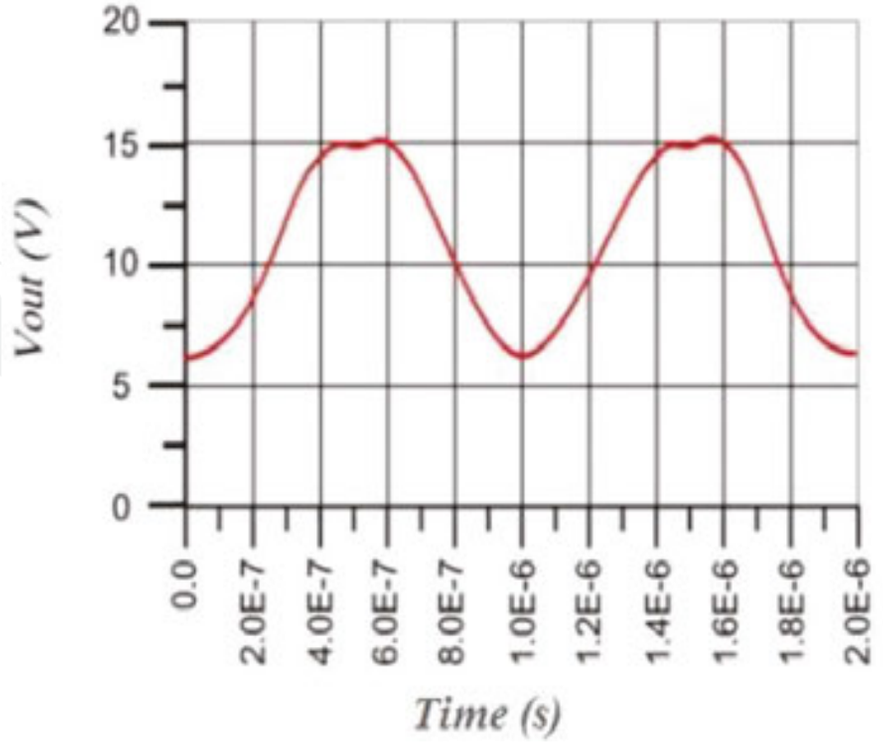

Figure 24. Temporal response the output voltage, for $V_{in} > V_c$.

5. An efficient architecture involving broadcast of RF power amplifiers

The main focus of this Section is to present an efficient in-house NTSC architecture that can works as an exciter with a central PC that controls various interfaces. With the setup of this electronic structure, it is possible to make a communication with different measurement equipment, and the levels generated by the exciter are sufficient to drive the power drawer to the nominal power 860 (Wps). All numerical codes of the central software that interfaced and controlled all equipment were written using both *Matlab* platform. For this design, the most important interfaces are the Serial *RS232*, *USB*, *GPIB*, and *LAN*, and the final software presents an easy-to-use interface that are strongly demanded currently in the production line of all modern RF architectures [7–10, 12–17, 23].

5.1. A wide class of important reports: principal measurements over the power amplifier

Figure 25 shows the amplifier we intend to make some experimental tests. This is a picture from a part of the power drawer that shows four RF power transistors, capable of delivering altogether 860 (Wps).

Typically, the operation of this device preserves the balanced configuration and has some similarity with other literatures as described previously. For the case that the setup has a correct operation, a wide class of different reports can be generated [20–22, 24, 36–42].

Hybrids structures were used to combine push–pull amplifiers, such that we should expect a difference in the current of the transistors, especially in the middle of the UHF band, when the coupled and the direct port present the largest dispersion from the ideal 3 dB value. The designer can use all reports to get enough background about the performance analysis of the amplifier under test, as well as to acquire a fine tuning of an amplifier that is being optimized using the same setup. At first, we shown in **Figure 26**, the current of each transistor recorded for each channel, in the entire UHF band.

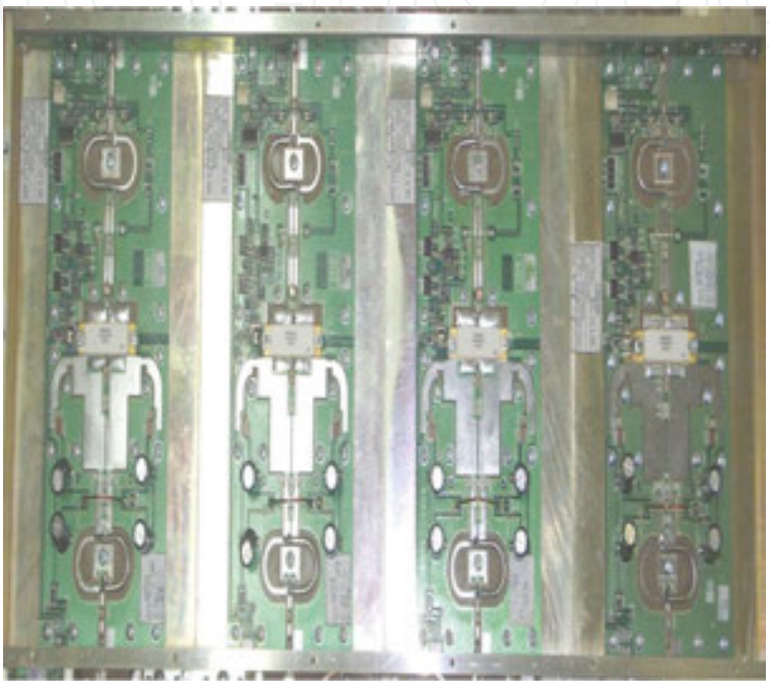

Figure 25. The RF architecture implemented for experimental tests with four power amplifiers with 860 (Wps).

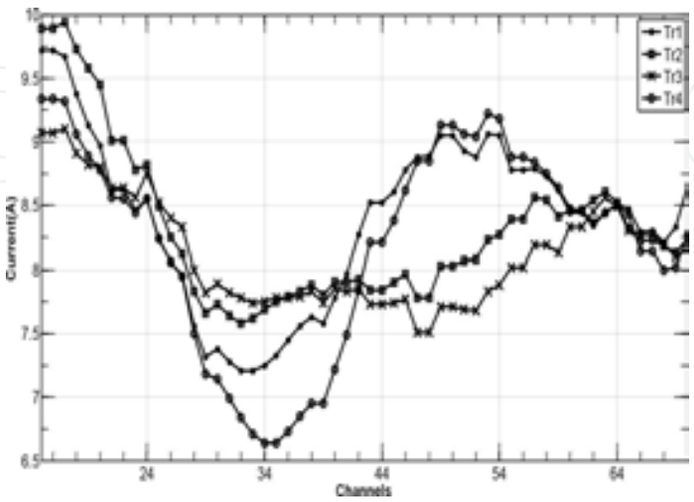

Figure 26. Currents of each transistor measured at nominal power for the UHF band (channels 14–69).

http://dx.doi.org/10.5772/63547

A 2D diagram in the entire UHF band for the temperature of each transistor is presented in **Figure 27**. Evidently, the transistors that were operating with less current due to the imperfect signal division of the hybrids presented lower temperatures, but the maximal ratings are important measures to verify the air cooling system of the drawer.

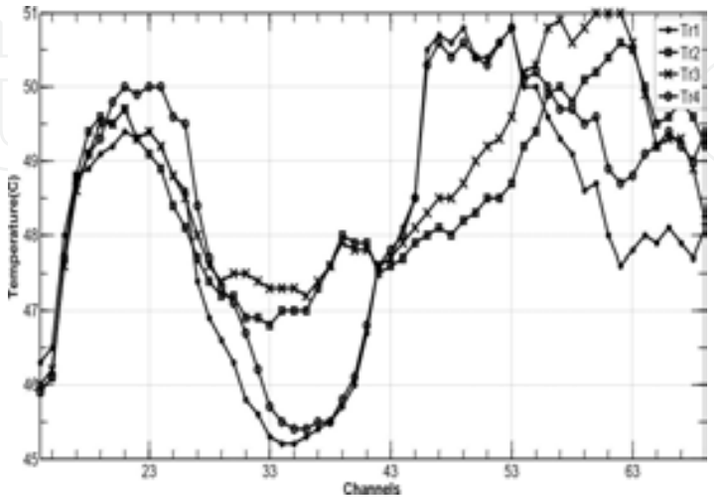

Figure 27. Temperatures of each transistor measured at nominal power for the UHF band (channels 14–69).

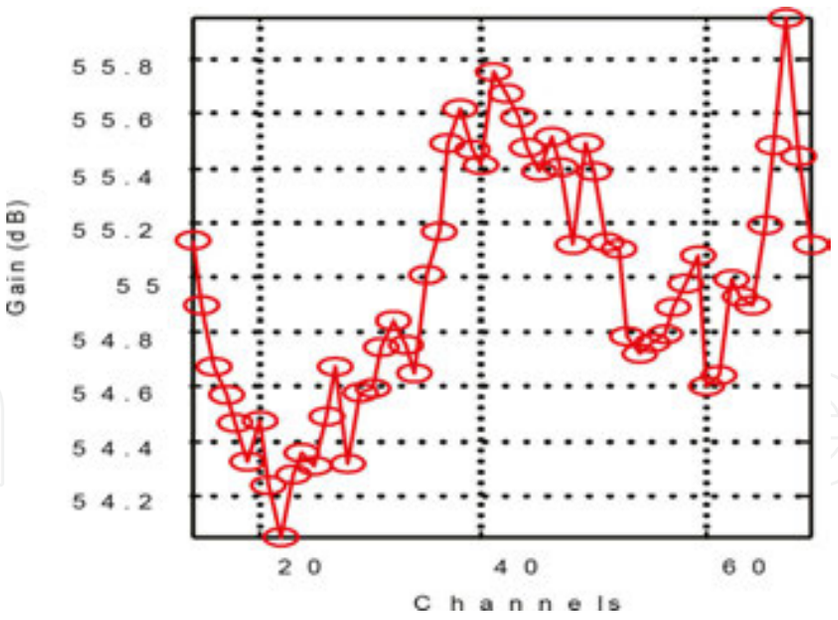

Figure 28. Plot of the gain (*dB*) for the UHF band (channels 14–69).

With this architecture, it is possible to perform a complete set of reports, as we can visualize in the graphic of **Figure 28** that shows the values of the Gain (*dB*) versus the UHF television channels (14–69), while **Figure 29** depicts the inter-modulation of 0% average power level (APL) black signal located at (−4.5) (MHz).

In order to consider the stress conditions generated by the amplifier by considering the signal that represents the highest output power generated by the device in an NTSC transmission, we must check the use of the APL 0% black signal. This experimental allows observe the *IMD* generated by the amplifier at the maximum output power in the entire band imposed for the operation of the device. Therefore, it is possible to plot both the lower side of the *IMD* (−4.5 MHz) and the upper side of the *IMD* (9 MHz), and we can detect a high asymmetry between the lower and the higher sides of the *IMD* frequencies.

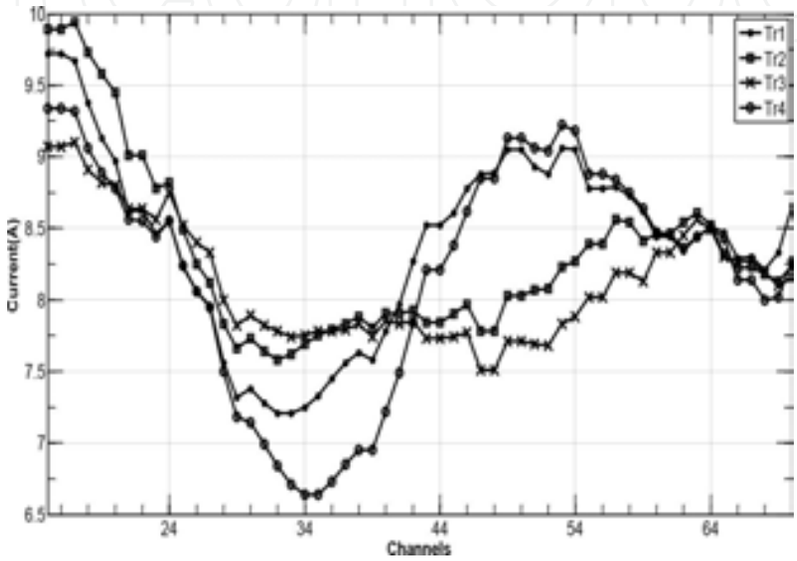

Figure 29. Plot of the inter-modulation (0%) APL black signal located at −4.5 (MHz), for the UHF band (channels 14–69).

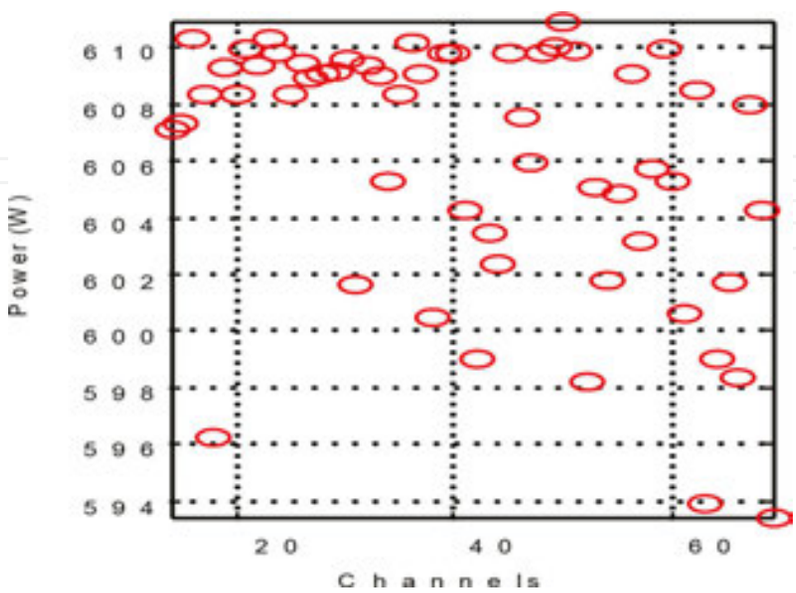

Figure 30. Plot of the (75%) red *Ramp* signal for the UHF band (channels 14–69).

http://dx.doi.org/10.5772/63547

If we taking into account that the human eye is sensitive to static noise intermixed in a red field, such that the *IMD* levels should be as low as possible in a good quality amplifier, it is important to get a 2D plot corresponding to the (75%) red *Ramp* test signal results for the same UHF television channels, which is represented in **Figure 30**.

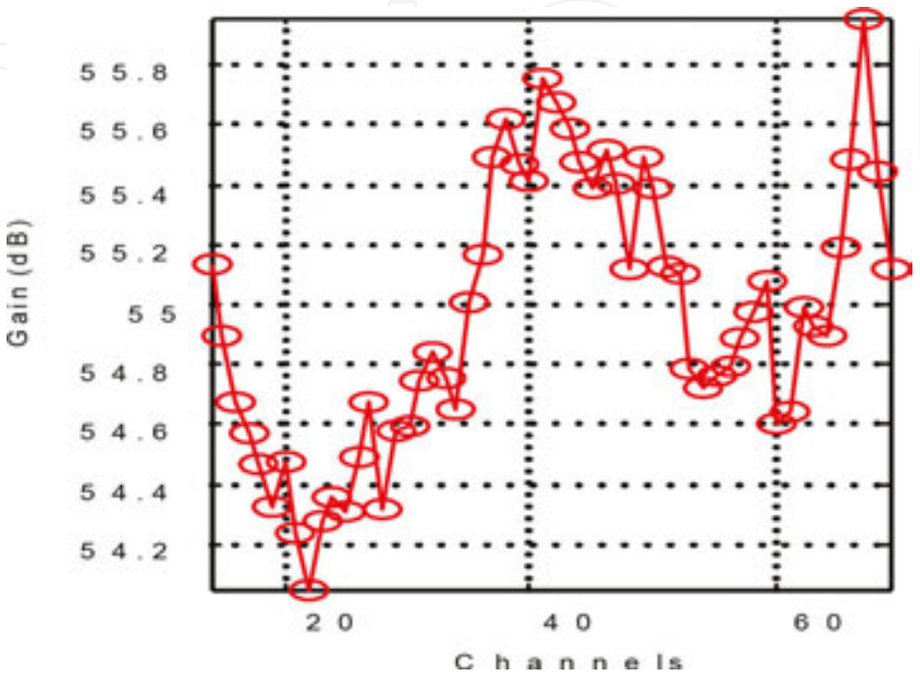

Figure 31. Plot of both local oscillator and the mirror signals for the UHF band (channels 7 14–69).

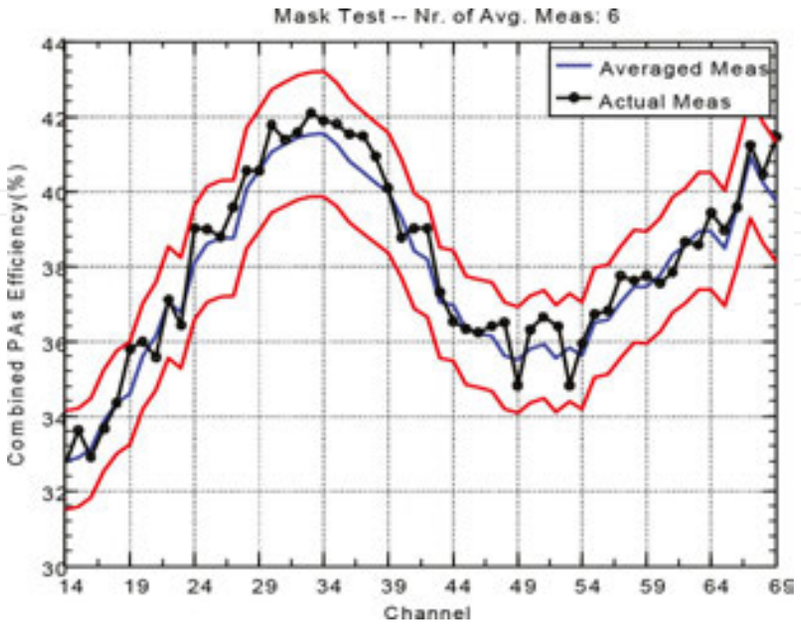

Figure 32. A statistical comparison of the combined PA's efficiency for validation of all measurement tests.

It is possible also to perform a graphic that corresponds the efficiency of the power drawer for the entire UHF band, since this test would indicate the RF power delivered over the total power consumed by the amplifier. Another important report is corresponding to the level of both local oscillator (LO) and the mirror signals as a function of the same channels of UHF television, which is plotted in **Figure 31**. This test ensures that the LO of the modulator and the mirror signals are low enough, which permit us the complete validation of this experimental test.

As a conclusion of all experimental measurements, it is really important to use all data available, which permit us not only to make some statistical comparisons as well as pass-fail tests were it is possible. This procedure presents a mean value of several results that were performed, such that it is possible to establish a comparison with the actual measurements and those ones we have made previously. If more tests are realized more precise, they become and the mean curve can be adjusted more conveniently, as it is being presented in **Figure 32** [22–26, 42–47].

Using this mean curve and upper and lower bounds, a defective piece can be easily identified and sent to repair if necessary. A good agreement can be observed for the amplifier tested in this graphic, and so the behavior of the amplifier was inside expectations.

5.2. Block diagram and the setup of the entire experimental hardware architecture

A block diagram corresponding to the flows of the signal for the implemented architecture is depicted in **Figure 33**. For both input and output signals, it will be necessary to check the system gain and to ensure that the output power is at the correct level, a set of instruments such as: Power Meters, USB2001, E4416B, Current Probe 34134A, and the 34401A Multimeter, in order to get the whole system that will be used to measure the drawer overall efficiency. The transistor currents were measured from the power drawer supply, and the temperatures were acquired from a sensor placed at the side of the transistor flange.

With the purpose of to maintain the exciter totally "*free of distortion*"; sometimes, we need to check and realize, the performance of both the local oscillator (LO) as well as the image suppression for each analyzed channel. An ESA spectrum analyzer can serve for this experimental procedure which permits also to detect inter-modulation levels of three different NTSC signals, namely 0% average power level (APL) black, 75% modulated red, and the modulated ramp.

In comparison with others commercial systems (e.g., Anritsu ME 7840A), this architecture is more flexible regarding the output power as well as all individual components. Besides of the RF structure being composed by several parts, these ones can be tuned for a single amplifier module of 220 (Wps) or a power drawer 860 (Wps), which permits that some parts can also be substituted by low-cost equivalent, as for example, power meters, current meters, attenuators, and couplers.

http://dx.doi.org/10.5772/63547

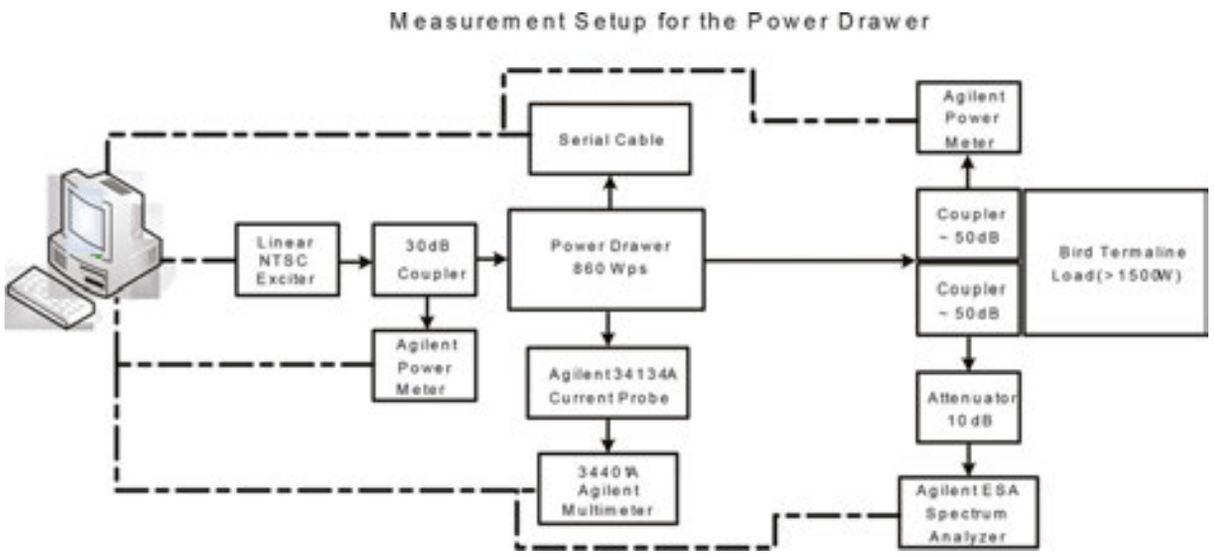

Figure 33. Design of the whole architecture for the measurement setup.

For the case that the architecture shown in **Figure 33** will be used for standard *ISDB-T* OFDM signals, some minor changes in software to measure inter-modulation distortions must be performed when the signal is applied to a power amplifier. In the references presented at the Introduction, a detailed study about *IMD* distortions caused by a power amplifier in an *ISDB-T* OFMD signal and also its peak-to-average ratio (*PAR*) characteristics is presented.

The whole architecture will serve for submit under test a wide class of power amplifiers. All reports generated in accordance with the performance analysis of each amplifier makes possible to implement a fine tuning of the device. Furthermore, it is possible to combine *push–pull* amplifiers, for the case that hybrids structures must be used, and we should expect a difference in the current of the transistors, especially in the middle of the UHF band, when the coupled and the direct port present the largest dispersion from the ideal 3 *dB* value.

Acquires a great importance the reports corresponding to the fluctuation of the temperatures of each transistor in the entire UHF band. Initially, we impose set all values of the Power (W) and the Gain (*dB*) versus the UHF television channels (14–69), in accordance with the inter-modulation of 0% APL black signal, for some specified frequencies. Typically, the use of the APL 0% black signal is due to the stress conditions generated in the amplifier, by considering that this signal represents the highest output power generated by the device for an NTSC transmission. This test allows the observation of the IMD effect generated at the maximum output power in the entire band imposed for the operation of the amplifier [48–52].

Finally, corresponding to the generation of inter-modulation reports that can be used in the analysis of PAR of digital signals, we should expect a sensible broadening in the domain of applications of the measurement architecture. An alternative option for this architecture is to use it for the validation of noise analysis as well as to validate some studies for uplinks for cognate radio structures made for a wide class of OFDM systems. In conclusion, a load capable of absorbing the amount of power generated by the amplifier under test is used as termination,

preceded by two couplers. The complete architecture implemented on a rack for all measurements can be visualized in **Figure 34**.

Figure 34. The whole architecture which contains all equipment used to perform all requirements measurements conveniently mounted on a rack.

The whole architecture presented in this Section can be used widely for the characterization of high-power amplifiers, and the structure was designed to be used in the production line of modern RF companies. Important parameters, such as gain, output power, inter-modulation distortion of different signals, efficiency, current, and temperature, can be measured in accordance with the intrinsic characteristics of a wide class of amplifiers. The RF electronic structure can generate very important reports that can be used to avail the performance of the amplifier under test, comparing it to other amplifiers already measured.

6. Conclusions

The theoretical research with experimental validation presented in this chapter was aimed primarily to introduce new technologies that can be used in modeling of nonlinear phenomena that attend intrinsically in the projects involving the power amplifiers used widely in the new industrial production lines of high-resolution digital systems of TV.

The competitiveness that is continuously imposed on the international scene demand that professionals involved with projects of new technologies keep always a updated vision of what can be more in terms of new emergency equipment should be projects for communication links using techniques in which the *Digital Signal Processing* (DSP), with high rates of transmission by making that information, regardless of its analog or digital form can get the link *Tx-Rx*

efficiently, with optimized time, protected against intrinsic noise in transmission, with a modern computing platform that allows not only to implement the codes are written in structures *Field-Programmable Gate Array* (FPGA), as well as all the simulations that can validate the theoretical approaches formulated, in addition to a safe protection of traffic information.

This demand of designers a vigilance on construction of versatile systems, extreme precision, so that the demands imposed on business sectors may be always being supplied in real time, which keeps the heated market, strengthening thus the companies that are on the line, in the discovery of new fronts in their diverse research lines of production. Constant challenges are always objectified targets to the engineers who are involved with projects of new technologies. The space in the international market is something that outlines as one of the fundamentals of the companies who engage seriously in new lines of production equipment used in the transmission and reception of signals in the wide area of Radio Frequency (RF).

We hope this set of theoretical and experimental approaches presented in this Chapter can be our modest contribution for the development of new technologies as well as can serve as a guide for many engineers with strong interests in this field of research.

Acknowledgements

We would like to thank the Institutions: Foundation of Studies and Projects, FINEP, RJ, for all financial support received for this research; Linear Equipamentos Eletrônicos S/A, one of the best Companies in Brazil that produces RF and Microwave equipments with high performance, where were developed all projects related with a wide class of HDTV transmitters architectures; São Paulo Research Foundation, FAPESP, SP, processes with ID: 2006/01655-7 and 2013/23431-7; Minas Gerais Research Foundation, FAPEMIG, MG, by all financial supports received by the authors; Brazilian Educational Ministry, CAPES, MCT, for the PhD scholarship studies developed by an author in Austria.

Author details

Daniel Discini Silveira[1], Marcos Paulo de Souza Silva[2], Marcel Veloso Campos[3] and Maurício Silveira[4*]

*Address all correspondence to: maur.silveira@gmail.com

1 Federal University, Ufjf, Juiz de Fora, Minas Gerais, Brazil

2 São Paulo's Electricity Company, CESP, São Paulo, Brazil

3 State University, Unimontes, Montes Claros, Minas Gerais, Brazil

4 Federal University, UFSCar, São Carlos, São Paulo, Brazil

References

[1] Vuolevi, J. and Rahkonen, T., Distortion in RF Power Amplifiers, Norwood, MA: Artech House, 2003.

[2] Maas, S.A., Nonlinear Microwave Circuits, Piscataway, NY: IEEE Press, 1988.

[3] Cripps, S.C., Advanced Techniques in RF Power Amplifier Design, Norwood, MA: Artech House, 2002.

[4] Kenington, P.B., High-Linearity RF Amplifier Design, Norwood, MA: Artech House, 2000.

[5] Pothecary, N., Feedforward Linear Power Amplifiers, Norwood, MA: Artech House, 1999.

[6] Lima, J.S. and Silveira, M., Medidas de desempenho em Sistemas 8-VSB e COFDM. In: Proceedings of the International Week of Telecommunication, 2002, National Institute of Telecommunication, Santa Rita do Sapucaí, MG, Brazil.

[7] Lima, J.S., Linearization of TV transmitters with IF pre-distortion, Telecommunication Journal, National Institute of Telecommunication, 1998, Vol. 1, Brazil.

[8] Mello, A.A., Rodrigues, H.D., Lima, J.S., Silveira, M., Pereira, W.N., Ribeiro, J.A.J., Linearization of the transmitter using digital pre-distortion. In: Proceedings of the IEEE APS-URSI (APS-URSI'02); 2002, San Antonio, TE, USA.

[9] Mello, A.A., Rodrigues, H.D., Lima, J.S., Silva, M.P.S., Silveira, M., Pereira, W.N., O uso da técnica de pré-distorção digital na linearização de amplificadores de potência em RF, In: Proceedings of the International Week of Telecommunications; 2002, National Institute of Telecommunication, Santa Rita do Sapucaí, MG, Brazil.

[10] Mello, A.A., Rodrigues, H.D., Lima, J.S., Silva, M.P.S., Silveira, M., Adaptive linearization using pre-distortion experimental results, Telecommunication Journal, National Institute of Telecommunication, 2004, Vol. 3, Brazil.

[11] Mello, A.A., Rodrigues, H.D., Lima, J.S., Silva, M.P.S., Silveira, M., An efficient Numerical Approach for the Linearization of Power Amplifiers, IEEE Journal Latin America, Vol. 2, 2, 2004.

[12] Silva, M.P.S., Silveira, M., et al., An efficient analysis of the performance of nonlinear devices using as a tool the software ADS. In: Proceedings of the IEEE of Word Congress on Engineering and Technology Education (WCETE'04), 2004, Guarujá, Brazil.

[13] Mello, A.A., Rodrigues, H.D., Lima, J.S., Silva, M.P.S., Silveira, M., A new numerical approach in the linear analysis of RF amplifiers. In: Proceedings of the IEEE 33rd European Microwave Conference (EuMC'03); 2003, Munich, Germany.

[14] Mello, A.A., Rodrigues, H.D., Silva, M.P.S., Silveira, M., Adaptive digital pre-distortion to reduce the power amplifier non-linearity. In: Proceedings of the IEEE APS-URSI (APS-URSI'03), 2003; Columbus, OH, USA.

[15] Clarke, K., Hess D., Communication Circuits: Analysis and Design, Krieger Publishing Co., 2nd ed., Malabar, FL, 1994.

[16] Kim, J. and Konstantinou, K., Digital predistortion of wideband signals based on power amplifier model with memory, Electronics Letters, 2001, Vol. 37, 23, pp. 1417–1418.

[17] Silveira, D.D., Gilabert, P.L., Lavrador P.M., Pedro J.C., Gadringer M., Montoro G., Bertran E., Magerl G., Improvements and analysis of nonlinear parallel behavioral models, Journal of RF and Microwave Computer-Aided Engineering, 2004. doi:10.1002/mmce.20385.

[18] Kenington, P.B., High Linearity RF Amplifier Design, New York, NY: Artech House, 2000.

[19] Fischer, W., Digital Video and Audio Broadcasting Technology. A Practical Engineering Guide, New York, NY: Springer, 2008.

[20] Pedro, J.C., Maas, S., A comparative overview of microwave and wireless power-amplifier behavioral modeling approaches, IEEE Transactions on Microwave Theory and Techniques, 2005, Vol. 53, 4, pp. 1150–1163.

[21] Cripps, S.C., Advanced Techniques in RF Power Amplifier Design, New York, NY: Artech House, 2002.

[22] Kenington, P.B., Analysis of instability in feed-forward loop, Electronic Letters, Vol. 33, 1997.

[23] Marmarelis, V.Z., Nonlinear Dynamic Modelling of Physiological Systems, Hoboken, NJ: J. Wiley & Sons, 2004.

[24] Cavers, J.K., Amplifier linearization using a digital pre-distorter with fast adaptation and low memory requirements, IEEE Transactions on Vehicular Technology, 1990, Vol. 39, 4, pp. 374–382.

[25] Lima, J.S., Silveira, M., The Weaver theoretical approach to generate some important TV digital signals for the transmission systems, In: Proceedings of the IEEE International Microwave and Optoelectronic Conference (IMOC'05), 2005, Belém, PA, Brazil.

[26] Rodrigues, H.D., Silveira, M., Ribeiro, J.A.J., Silva, D.G., Complex filtering for generation of SSB and VSB signals, In: Proceedings of the IEEE Asia Pacific Microwave Conference, (APMC'05), 2005, Hong Kong, China.

[27] Sedra, A.A., Smith, K.C., Microeletrônica, 5th ed., São Paulo: Makron Books, 2004.

[28] Cripps, S.C., RF Amplifiers for Wireless Communications, New York, NY: Artech House, 1999.

[29] Vuolevi, J., Analysis, measurement and cancellation of the bandwidth and amplitude dependence of intermodulation distortion in RF power amplifiers, Lecture Notes, Department of Electrical Engineering, University of Oslo, Blindern, Oslo, 2001.

[30] Wang, H., Bao, J. Wu, Z., Comparison of the Behavioral Modeling for RF Power Amplifier With Memory Effects, IEEE Microwave and Wireless Components Letters, 2002, Vol. 19, 3, pp. 179–181.

[31] Cantrell, W.H., Davis, W.A., Amplitude modulator utilizing a high-Q class-E DC-DC converter, In: Proceedings of the IEEE MTT-S Microwave Symposium Dig. (MTT-S'03), June 2003, Vol. 3, pp. 1721–1724.

[32] Elnady, A., An efficient current regulator for multilevel voltage source converter based on a simple analog control circuit, Journal of Circuits, Systems and Computers, 2013, Vol. 22, 4, pp. 1–21, doi:10.1142/S021826613500230.

[33] Hung, T.P., Metzger, A.G., Zampardi, P.J., Iwamoto, M., Asbeck, P.M., Design of high-efficiency current-mode class D amplifiers for wireless handsets, IEEE Transactions on Microwave Theory and Techniques, 2005, Vol. 53, pp. 144–151.

[34] Campos, M.V., Silveira, M., An efficient analytical approach for the non-linear analysis of RF amplifiers implemented with the FET structures, In: Proceedings of the IEEE Asia Pacific Microwave Conference, (APMC'05), Dicember 2005, doi:10.1109/APMC.2005.1606219.

[35] Campos, M.V., Silveira, M., An original approach of the effect source resistance for FET devices, In: Proceedings of the IEEE Asia Pacific Microwave Conference, (APMC'08), Dicember 2008, doi:10.1109/APMC.2008.4958523.

[36] Sevic, J.F., Statistical characterization of RF power amplifier efficiency for CDMA wireless communication systems, In: Proceedings of the IEEE Wireless Communications Conference, 1997, p. 110–113, doi:10.1109/WCC.1997.622258.

[37] GPIB tutorial, Available from: http://cp.literature.agilent.com/litweb/pdf/04396-90063.pdf.

[38] Duffy, D.G., Advanced Engineering Mathematics with Matlab, 3rd ed., New York, NY: CRC Press, 2010.

[39] Tektronix, Television measurements manual for NTSC system, Available from: http://www.tek.com/document/primer/television-measurements-ntsc-systems.

[40] Silveira, D.D.; Lima, J.S.; Silveira, M.; Dissect PA distortion from OFDM signals, Microwaves & RF Magazine, 2010; Vol. 01, pp. 88–94.

[41] Bermudez A. et al., Mathematical Models and Numerical Simulation in Electromagnetism, 1st ed., New York, NY: Springer Publisher, 2014.

[42] Varahram, P., Ali, B.M., Peak-to-average power ratio reduction and digital pre-distortion effects in power amplifiers in OFDM systems; International Journal of Communication Systems, 2012, Vol. 25, pp. 543–552, doi:10.1002/dac.1282.

[43] Wen, J.H., Lee, S.H., Cheng, C.H., SLM-based PAPR reduction method using partial data circulation and side information insertion in OFDM systems; International Journal of Communication Systems, 2009, Vol. 22, pp. 87–100, doi:10.1002/dac.v22:1.

[44] Tu, H.C., Chiu, C.C. A novel search method to reduce PAPR of an OFDM signal using partial transmit sequences; International Journal of Communication Systems, 2007, Vol. 20, pp. 147–157.

[45] Jeng, S.S., Chen, J.M., Chang, P.H., A low-complexity companding technique using Padé approximation for PAPR reduction of an OFDM system, International Journal of Communication Systems, 2011, Vol. 24, pp. 1467–1479, doi:10.1002/dac.1231.

[46] Rozic, N., Radic, J., Theoretical analysis of iterative signal reconstruction for impulsive noise mitigation in OFDM systems, International Journal of Communication Systems, 2010, Vol. 23, pp. 1467–1479, doi:10.1002/dac.1058.

[47] Lu, Q.; Peng, T., Wang, W., Wang, W., Hu, C., Utility-based resource allocation in uplink of OFDMA-based cognitive radio networks, International Journal of Communication Systems, 2010, Vol. 23, pp. 1467–1479, DOI: 10.1002/dac.1070.

[48] Yong, J.J., Hyung, W.K., Hong, T.K.; Gi, H.R., Ji,Y.C., Kim, K., Soo, E.S., Byungdu, O., A highly efficient CDMA power amplifier based on parallel amplification architecture; IEEE Microwave and Wireless Components Letters, 2004, Vol. 14, pp. 401–403, doi: 10.1109/LMWC.2004.832050.

[49] Karthaus, U., Sukumaran, D., Schmidt, L., Ahles, S., Wagner, H., A 45 dBm balanced power amplifier module based on four fully integrated Doherty PA MMICs. A scalable solution for cellular infrastructure active antenna systems, In: Proceedings of the IEEE 42nd European Microwave Conference (EuMC'12), 2012, Vol. 1, pp. 1027–1030.

[50] Osman, A.F., Noh, N.M., Wideband LNA design for SDR radio using balanced amplifier topology, In: Proceedings of the IEEE 4th Asia Symposium on Quality Electronic Design (ASQED'02), 2012, Vol. 1, pp. 86–90, doi: 10.1109/ACQED.2012. 6320481.

[51] Ji, Y.P.; Burger, J., Titizian, J., UHF band long-pulse radar power amplifiers using push-pull and balanced configurations; In: Proceedings of the IEEE International Microwave Symposium, (MTT-S'07), 2007, Vol. 1, pp. 15–18, DOI: 10.1109/MWSYM.2007.380206.

[52] Jack, K., Video Demystified: A Handbook for the Digital Engineer, 5th Ed., New York, NY: Elsevier, 2011.

IntechOpen